DOI 10.48612/fpg/92rg-6t7h-m4a2

УДК 551.465

© *V. G. Gnevyshev*[1], *V. S. Travkin*[2], *T. V. Belonenko*[2]*, 2023

© Translation from Russian: *E. V. Rykova*, 2023

[1]Shirshov Institute of Oceanology, Russian Academy of Sciences, 36 Nakhimovsky Prosp., Moscow, 117997, Russia
[2]St. Petersburg State University, 7–9 Universitetskaya Emb., St. Petersburg, 199034, Russia
*btvlisab@yandex.ru

# TOPOGRAPHIC FACTOR AND LIMIT TRANSITIONS IN THE EQUATIONS FOR SUB-INERTIAL WAVES

Received 29.09.2022, Revised 08.11.2022, Accepted 08.12.2022

**Abstract**

In this paper, sub-inertial waves propagating on the Kuril shelf and the oceanic trench are considered. Against the background of a historical review of the beginning of the study of topographic waves and the appearance of relevant terms, a description of the features of wave propagation and the derivation of the main dispersion equations are given. We show that all variants of the topographic solutions presented in the article are basically based on the same dispersion relation: this is the dispersion relation for Rossby topographic waves. Two separate classes of localized solutions have been constructed: one is for the shelf, and the second, in fact, is also for the shelf, but which is commonly called trench waves. We demonstrate that the transverse wave number for trench waves is not independent, as for shelf waves, but is a function of the longitudinal wave number. In other words, Rossby topographic waves are two–dimensional waves, while shelf waves are quasi-one-dimensional solutions. The analytical novelty of the work consists of the fact that we can make crosslinking of trench and shelf waves. This fact was not presented in previous articles on this topic.

**Keywords**: shelf, ocean trench, topographic waves, shelf waves, trench waves, crosslinking solutions

© *В. Г. Гневышев*[1], *В. С. Травкин*[2], *Т. В. Белоненко*[2]*, 2023

© Перевод с русского: *Е. В. Рыкова*, 2023

[1]Институт океанологии им. П.П. Ширшова РАН, 117997, Россия, Москва, Нахимовский проспект, 36.
[2]Санкт-Петербургский государственный университет, 199034, Санкт-Петербург, Россия, Университетская наб., 7–9, г.
*btvlisab@yandex.ru

# ТОПОГРАФИЧЕСКИЙ ФАКТОР И ПРЕДЕЛЬНЫЕ ПЕРЕХОДЫ В УРАВНЕНИЯХ ДЛЯ СУБИНЕРЦИОННЫХ ВОЛН

Статья поступила в редакцию 29.09.2022, после доработки 08.11.2022, принята в печать 08.12.2022

**Аннотация**

Рассматриваются топографические субинерционные волны, распространяющиеся на шельфе и океаническом желобе. На фоне обзора истории исследования топографических волн и появления соответствующих терминов авторы дают описание особенностей распространения этих волн и вывод основных дисперсионных уравнений. Показано, что все варианты представленных в статье решений в основе своей базируются на одном и том же дисперсионном соотношении — это дисперсионное соотношение для топографических волн Россби. Построены два класса локализованных решений: одно для шельфовых волн, второе, фактически, тоже шельфовое, но его принято называть желобовыми волнами. Показано, что для желобовых волн поперечное волновое число не является независимым, как для шельфовых волн, а является функцией от продольного волнового числа. Другими словами, топографические волны Россби — это всегда двумерные волны, в то время как шельфовые волны представлены квазиодномерными решениями. Аналитическая новизна работы состоит в том, что в ней удалось произвести сшивки желобовых и шельфовых волн, которые ранее отсутствовали в работах по данной тематике.

**Ключевые слова:** шельф, океанский желоб, волны топографические, шельфовые, желобовые, сшивки решений

Ссылка для цитирования**:** *Гневышев В.Г.*, *Травкин В.С.*, *Белоненко Т.В.* Топографический фактор и предельные переходы в уравнениях для субинерционных волн // Фундаментальная и прикладная гидрофизика. 2023. Т. 16, № 1. С. 8–23. doi:10.48612/fpg/92rg-6t7h-m4a2

For citation: *Gnevyshev V.G., Travkin V.S., Belonenko T.V.* Topographic Factor and Limit Transitions in the Equations for Sub-inertial Waves. *Fundamental and Applied Hydrophysics.* 2023, 16, 1, 8–23. doi:10.48612/fpg/92rg-6t7h-m4a2

## 1. Introduction

In recent years, much research has appeared that studies various classes of sub-inertial waves in the ocean in areas characterized by significant changes in bottom topography (see, for example, [1–5]). For these ocean areas, wave energy capture is observed by huge topographic changes. Abrupt depth changes in the open ocean lead to the appearance of "topographic" waves, which are similar in nature to the shelf waves formed in the zone of the shelf-continental slope [6]. The comparative analysis of the contribution of various factors to the dispersion equations shows that the topographic factor is dominant [2–5, 7, 8]. Shelf waves are the most important type of sub-inertial oscillations, which plays an important role in the variability of the ocean level in the synoptic frequency range [6, 9].

In the fields of deep-sea trenches, another type of sub-inertial oscillation is formed, the propagating of which along the ocean side of the trench forms a system of trench waves. The term "trench waves" was first used by Mysak et al. [10] to study sub-inertial waves propagating in ocean trenches (Kuril, Japanese, Japanese-Kuril, Chilean, Peruvian). In the mathematical model of trench waves, two-dimensional topography is assumed to be uniform along the slope of the trench and has terminal scales of transverse variability.

To describe linear trench waves, a mathematical model is used, which is based on the line Schrödinger equation with additional boundary conditions that lead to quantization of the transverse wave number. The solution is constructed in a trigonometric form (sine), localized across the topographic feature, and a monochromatic plane wave traveling along the topographic feature — the slope of the trench. Note that the solution of the type "Kelvin double wave", for which two exponents are used in the topographic profile, is not considered in the trench wave model [10].

If the two-dimensional derivative of the shelf depth is constant, then mathematically the problem allows us to analyze the boundary problem in general form and formulate certain theorems of the spectral problem [6]. Solutions to this problem are called "shelf waves" [11].

If the two-dimensional derivative of the shelf depth changes a sign when moving away from the shore (ocean trench), then the mathematical analysis is significantly complicated. For trench-type topography, particular classes of piecewise smooth analytical solutions are constructed, which are conventionally called "trench waves". A feature of many ocean trenches is their close position to the coastline, thereby combining the shelf and continental slope areas and adjoining the inside of the trench (Figure 1). In the future, we will call the inner part of the trench, consisting of the shelf and the continental slope, reaching the maximum depth of the trench, "trench shelf". The oceanic side of the trench has less variability in depth and, as a rule, greater steepness [12]. Therefore, in the construction of the mathematical model of trench waves, the entire physical semiinfinite space is conditionally divided into three regions: 1) the trench shelf where the depth of the ocean increases; 2) the oceanic part of the trench, where the depth of the ocean decreases and the derivative of the function describing the depth changes the sign; 3) an open ocean, where the depth of the ocean is constant and finite.

Since only sub-inertial oscillations are considered trench wave model [10], the Earth's rotation rate is considered constant (there is no β-effect) and there are no shear flows, then the solution is always decaying exponentially in the open part of the ocean, and this solution is sometimes called "exponential tail".

We will consider wave movements on the $f$-plane, i.e.

$$f = \text{const}. \tag{1.1}$$

The consistency of the Earth's rotation rate destroys waves with frequencies less than the frequency of rotation of the Earth itself. Thus, in the open part of the ocean, sub-inertial wave oscillations are suppressed. This fact was first noted by Longuet-Higgins [13, 14].

In addition, the trench wave model [10] examines for sub-inertial oscillations with spatial scales of hundreds of kilometers, but does not take into account the β-effect in the open part of the ocean, i.e. a strictly closed wave system is built, and Rossby waves falling on the shelf from the open part of the ocean are actually excluded from the problem. The latter is the main shortage of this model. According to the theory [10, 11, 15], trench waves can be represented in the form of two particular solutions: 1) shelf waves: the solution is localized on the shelf part of the trench, while in the direction from the shelf towards the open ocean this solution can be represented

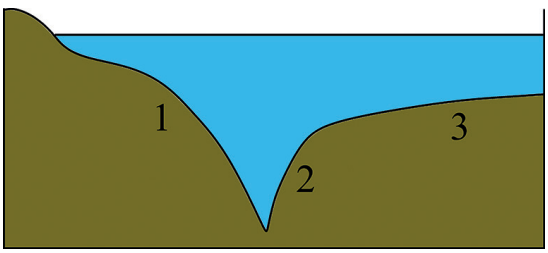


**Fig. 1**. Profile of the oceanic trench: 1 — trench shelf (shelf + continental slope), 2 — oceanic part of the trench, 3 — open ocean

as oscillation-attenuation-attenuation; 2) trench waves: the solution is localized on the oceanic part of the trench, this solution can be imagined as attenuation–oscillation–attenuation. A fundamentally important point is that in at least one part of the profile in the trench wave model (recall that there are three parts of the profile — trench shelf, trench, open ocean) there must be an oscillatory solution, moreover, there must be a sine in the solution, in the other two must be a damped exponential function, and in the open part of the ocean an exponential tail [10]. In this case, as shown in the paper [10], the shelf part of the solution is asymptotically stitched with the Buchwald and Adams shelf wave [16], if the model eliminates the oceanic trench part of the topography and turns its width to zero. However, acting similarly for the chute part of the solution and rushing the width of the already shelf part of the topography to zero, the authors [10] could not sew the chute solution with the inner shelf wave of Buchwald and Adams. They simply did not analyze this fact, citing little interest in this class of solutions. As a result, the question: of whether trench waves are sewn or not sewn [10] with the decision of Buchwald and Adams [16] remaining open. In this work, we will eliminate this drawback and show that the trench solution [10] is sewn together with the inner shelf wave of Buchwald and Adams. To do this, it is necessary not to zero the width of the shelf part of the topography (the trench shelf), placing the solid wall in the center of the trench, as it was done [10], but, on the contrary, to push it infinitely far. As a result, the analysis of trench waves becomes logical and complete.

Thus, we formulate the purpose of the study as follows: we will show that the solution of the "trench waves" is asymptotically sewn together with the topographic and internal topographic waves of Buchwald and Adams. The specificity consists in the method of the limit transition, namely: to sew the oceanic part of the trench solution of Mysak et al. [10] with the inner shelf wave of Buchwald and Adams, you need to direct the trench part of the solution to zero, or, conversely, direct the width of the trench to infinity while simultaneously striving for the steepness of the shelf to zero. And to crosslink the trench wave with the internal topographic wave of Buchwald and Adams, you also need to endlessly move the border, expanding the shelf area and turning zero shelf steepness.

This work is constructed as follows. In the second section, we give the basic equations and give the dispersion relations for the Rossby topographic waves. Next, we see into question from simple to complex: first in the third section, we give the Buchwald and Adams solution, which subsequently becomes the asymptotics of the more complex solution of Mysak et al. Then, in the fourth section, we give this solution [10] for trench waves, simultaneously eliminating many misprints in their work, and we sew successfully the solution [10] asymptotically with the Buchwald and Adams solution. As a result, we prove that the Buchwald and Adams solution is the asymptotics of the solution of Mysak et al. [10].

The central idea of the article, which is discussed in the next three sections (5–7), is the statement that all variants of the topographic solutions presented in the article are based on the same dispersion relation — this is the dispersion relation for topographic Rossby waves. We show that this approach greatly simplifies the perception of the different topographic models discussed in the work.

## 2. Formulation of the problem. Basic equations

The theoretical basis for describing trench waves is linearized barotropic equations of shallow water in the rigid-lid approximation taking into account the topography [6, 10]:

$$u_t - fv + \rho^{-1} p_x = 0, \tag{2.1}$$

$$v_t + fu + \rho^{-1} p_y = 0, \tag{2.2}$$

$$(Hu)_x + (Hv)_y = 0. \tag{2.3}$$

Following the work [10], we assume the geostrophic approximation, thereby filtering out the high-frequency continuous spectrum of Poincaré waves, as well as edge waves:

$$u = -\Psi_y / H,\ v = -\Psi_x / H. \tag{2.4}$$

The following designations are used: $u$ and $v$ are the velocity components in the $x$ and $y$ directions, $\Psi$ — current function, $H$ is the depth, $p$ is the pressure, $\rho$ is the water density, and $f$ is the Coriolis parameter. The classical right coordinate system is adopted, axes $x$ and $y$ are directed across the trench (away from the coast ($x = -L_1$)) and along the trench, respectively.

Substituting (2.4) in (2.1) and (2.2) (equation (2.3) is performed automatically) and considering solutions of wave nature along the topographic feature (trench slope)

$$\Psi = \Psi(x) \exp i\left(k\, y - \omega t\right), \tag{2.5}$$

we get the following linear homogeneous one-dimensional equation:

$$\left(\frac{\Psi_x}{H}\right)_x + \left[\frac{f\,k}{\omega}\left(\frac{1}{H}\right)_x - \frac{k^2}{H}\right]\Psi = 0\,, \tag{2.6}$$

where $k$ — is the longitudinal component of the wave number, which is strictly real and, according to [10], strictly positive, ω — is the frequency of the wave, which is also real and can take both positive and negative values. Accordingly, depending on the sign, different directions of the phase velocity are obtained. Note that, unlike this approach, in the monograph [6], on the contrary, the ω is always positive, but the wave number k can take both positive and negative values. Therefore, different directions of wave propagation — northeast or southwest — are achieved by a different sign of wave number.

The cross-linking conditions at $x = 0$ (the center of the trench is the point of maximum depth on the profile) и $x = L_2$ (the boundary of the trough on the side of the open ocean)

$$[\Psi] = 0,\, x = 0,\, x = L_2, \tag{2.7}$$

$$\left[\frac{\Psi_x + \left(f\,k/\omega\right)\Psi}{H}\right] = 0, \quad x = 0, \quad x = L_2\,. \tag{2.8}$$

Condition (2.8) for a topography model with a continuous function takes the form

$$[\Psi_x] = 0,\, x = 0,\, x = L_2. \tag{2.9}$$

Also, in the shelf area, the impermeability boundary condition is set at the point $x = -L_1$ [10]:

$$[\Psi] = 0,\, x = -L_1 \tag{2.10}$$

and decaying condition at infinity:

$$\Psi \to 0,\, x \to \infty. \tag{2.11}$$

***Dispersion relation for the Rossby topographic wave on the exponential profile of the topography***

The classical substitution $\Psi = H^{1/2}$ in equation (2.6) can remove the first derivative [3, 9] and bring the above equation to the equation with the classical harmonic oscillator potential. The most successful and easy-to-analyze oceanic trough model is one with an exponential topography profile under the analytical approach and one with a stepped profile for numerical counting. There are other special cases of parameterization of the topography when it is possible to obtain non-reflective solutions [17, 18], and solutions in terms of degenerate hypergeometric functions [19].

For the classical topographic Rossby wave on the exponential profile of topography $H = H_0\exp(-x/L)$, $L$ is the shelf width, a solution is sought in the form of $\Psi = H^{1/2}\exp\left[i\left(k_1 x + k_2 y - \omega t\right)\right]$, where $k_1$ and $k_2$ are the transverse (across the trench) and longitudinal wavenumbers. Then the dispersion relation has the form [3, 9]:

$$\omega = \frac{-\left(\beta_0 + f/L\right)k_2}{k_1^2 + k_2^2 + 1/4L^2}\,, \tag{2.12}$$

where $\beta_0$ is the β-plane parameter.

The main idea of this work is that all varieties of subinertial topographic waves, including shelf and trench waves, follow precisely from this dispersion relation. And therefore, we propose to call the relation (2.12) the general dispersion relation on the exponential profile of topography (see also [4, 5]).

Historically, the first to construct an analytical model of subinertial topographic waves were Buchwald and Adams [16]. In their work, they analyzed two qualitatively different models of topographic waves: shelf waves and internal shelf waves. The principal difference between an internal shelf wave and a conventional shelf wave is the presence of an infinitely extended ocean of finite depth. This additional degree of freedom leads to the appearance of a certain feature in the behavior of the 0-mode, the analysis of which becomes extremely sensitive in the long-wave limit. The latter can be explained by the fact that the first mode either passes into a Kelvin double wave, or both waves have close dispersion curves in the long wave range. Looking ahead, we note that Buchwald and Adams saw certain difficulties in the limiting transition and considered its different options.

At the same time, Longuet-Higgins [13] conducts an extremely laborious analysis using higher-order decompositions to achieve the physical correct behavior of the frequency (the tendency of the frequency to zero when striving for zero, and not to the wavenumber constant). Other authors, in particular, [6, 10, 11] take a different path using numerical counting, and show smooth dispersion curves, including for the first mode. This approach does not mean that the analysis applied is incorrect, but rather indicates that different options are possible in the long-wave limit, and the result depends on what exactly the author is trying to find, given the scheme by which the boundary problem is numerically considered.

We move on to the description of the first and simplest model of topographic Rossby waves.

### 3. Buchwald and Adams shelf waves

The topography in the model [16] is taken in the following exponential form (see Fig. 2):

$$\begin{aligned} H_1 &= H_0 \exp(2bx), \quad 0 < x \le 1, \\ H_2 &= H_0 \exp(2b), \quad x > 1. \end{aligned} \tag{3.1}$$

We are looking for a solution in the following form

$$\begin{aligned} \Psi_1 &= A \sin m\, x \exp b(x-1), \quad 0 < x < 1, \\ \Psi_2 &= A \sin m \exp\left[-k(x-1)\right], \quad x \ge 1, \end{aligned} \tag{3.2}$$

where we believe $k > 0$. Then the dispersion relation (2.12) will take the form

$$\omega = \frac{-2f\ b\ k}{k^2 + m^2 + b^2}. \tag{3.3}$$

The wave amplitude in this case decays exponentially at the same rate on both sides of the break. Further, using cross-linking derivatives of functions, we obtain a condition for a transverse wavenumber:

$$\tan m = -\frac{m}{k+b}. \tag{3.4}$$

Further analysis will consider the sewing together of shelf and trench waves.

#### *Buchwald and Adam's internal shelf waves*

The trench wave model [10] assumes that the shelf width is finite and that the shelf near the shore extends to a finite depth. However, if we assume that the left boundary of the model has finite depth and is moved to infinity, then the boundary condition (2.10) is replaced by the attenuation criteria (2.11). This type of topography is called "rapid underwater slope" or simply "underwater slope" ([9], paragraph 24, page 311). In the model, the approach of the "rigid lid" is taken, while considering waves with lengths less than the barotropic Rossby radius. The phase associated with each of its eigenfunctions propagates so that shallow water remains on the right (in the northern half-globe). It can also be shown that these waves have dispersion. As shelf width approaches zero, higher modes are reduced to steady currents.

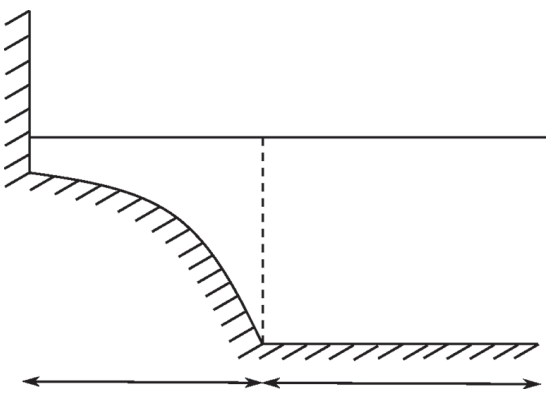

**Fig. 2**. Topography profile in Buchwald and Adam's model [16]

Following [16], we assume the following exponential topography model (Fig. 3):

$$\begin{aligned} H_1 &= h_1, \quad x \le 0, \\ H_2 &= h_1 \exp 2bx, \quad 0 \le x \le L_2, \\ H_3 &= h_1 \exp 2bL_2, \quad L_2 \le x < \infty. \end{aligned} \tag{3.5}$$

A solution is sought as follows:

$$\begin{aligned} \Psi_1 &= A_1 \exp(|k|\, x), \quad x \le 0, \\ \Psi_2 &= (A_2 \sin mx + A_3 \cos m\, x) \exp(bx), \quad 0 \le x \le L_2, \\ \Psi_3 &= A_4 \exp\left(-|k|\,(x - L_2)\right), \quad L_2 \le x < \infty. \end{aligned} \tag{3.6}$$

Again, using the dispersion relation for Rossby topographic waves, we obtain

$$\omega_n = \frac{-2f\ b\ k}{k^2 + l_n^2(k) + b^2}, \quad n = 1, 2, \ldots \tag{3.7}$$

From the conditions of crosslinks, we get the following condition for the definition $l_n(k)$:

$$\tan L_2 l_n = -\frac{2l_n|k|}{l_n^2(k) + b^2 - k^2}, \tag{3.8}$$

where $n$ — mode number.

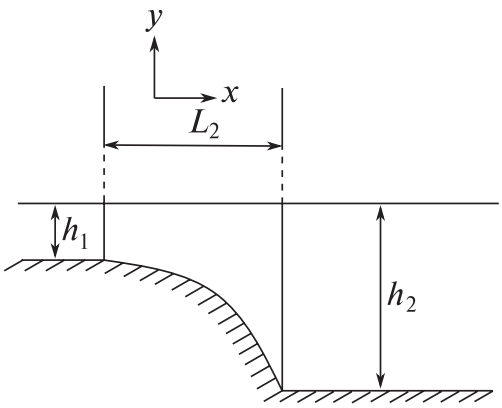


**Fig. 3**. Buchwald and Adam's topography model [16]

The analysis performed in the study [16] shows that the internal shelf waves practically coincide with the "ordinary" shelf waves, except for the 0-mode. The 0-mode of internal shelf waves has a certain specificity: its internal transverse wave number $l$ at small longitudinal wave numbers $k$ becomes virtual $l = i\,l_0$. Accordingly, equation (3.8) takes the form:

$$\tanh L_2 l_0 = \frac{2l_0|k|}{b^2 - l_0^2 - k^2}. \tag{3.9}$$

At the same time, the 0-mode frequency tends not to zero, as it happens in all other modes of topographic Rossby waves, but to the Earth's rotation frequency [16], which looks somewhat strange. Looking ahead, we note that Longuet-Higgins [13, 14] received a different result, and below we will show it. When divergence is taken into account, the frequency, as in many physical models, tends to zero, and the result is classical long waves. In the limit transition, when the width of the topographic feature tends to zero: $L_2 \to 0$, $b \to 0$, $bL_2 = 1/2\ln(H_1/H_3)$ this 0-mode, according to [16], passes into a divergence-free double Kelvin wave. For this mode, the decision over the topographic feature is no longer sinusoidal, but exponential. The term "Kelvin double wave" belongs to Longuet-Higgins [14].

However, and this is fundamentally important: the Kelvin double wave appears in the problem of internal shelf waves precisely as the limit transition of the 0-mode when moving to the type of topography in the form of a step and has nothing to do with the trench waves of Mysak et al. Note also that a characteristic scale for the 0-mode appears in the problem: $k_0 = \left(\sqrt{1 + b^2 L_2^2} - 1\right) / L_2$. This is the scale of the solution change in the 0-mode when the sinusoidal solution over the trench goes into a double exponential, i. e. Kelvin double wave. Below you will see that a close scale will be discussed in the next section. For the Kuril trench, for example, the value $bL_2 = 0.2332$, (see Table 1 [10]); wavelength calculations give a wave number $k_0 = 5 \times 10^{-4}$ km$^{-1}$, which corresponds to a wavelength of approximately 13,000 km. This is too large a value, and the appearance of instability is purely theoretical.

### 4. Mysak trench waves

In trench waves of Mysak et al. [10], the trench solution is highly localized above the topographic feature only from the shelf side. The value of the proper function on the shore has the order $10^{-3}$ of the value above the topography [6]. Therefore, for it, replacing the left leakage boundary condition with attenuation physically should not have a significant effect. For a trench wave, the presence of an infinitely extended open ocean of finite depth plays a more important role.

This model considers a more complex configuration, which essentially consists of two types of waves. It combines the shelf waves and the internal shelf waves of Buchwald and Adams [16]. Next, following the work [10], we assume the following exponential model of the trench:

$$\begin{aligned} H_1 &= H_0 \exp 2\alpha x, \quad -L_1 \le x \le 0, \\ H_2 &= H_0 \exp(-2\beta x), \quad 0 \le x \le L_2, \\ H_3 &= H_0 \exp(-2\beta L_2), \quad L_2 \le x < \infty. \end{aligned} \tag{4.1}$$

We have for the Kuril trench (see [10], Table 1): $H_0$ = 8.25 km, $L_1$ = 185 km, $L_2$ = 55 km, $\alpha = 0.95 \times 10^{-2}$ km$^{-1}$, $\beta = 4.24 \times 10^{-3}$ km$^{-1}$, $a = \alpha L_1 = 1.75$, $b = \beta L_1 = 0.784$, $r = L_2 / L_1 = 0.297$.

The topography profile is continuous, however, the derivative of the topography profile suffers a break. Therefore, a solution for the current function is sought on the class of piecewise smooth functions using the crosslinking conditions at $x = 0$ and $x = L_2$. The result obtained in work [10] can be formulated as follows: a solution satisfies automatically the condition (2.8) in the form

$$\begin{aligned}
&\Psi_1 = A\sin m(x + L_1) \qquad \alpha x \quad -L_1 \le x \le \\
&\Psi_2 = \left(B\sin lx + A\sin mL_1\cos lx\right)\exp(-\beta x), \quad 0 \le x \le L_2, \\
&\Psi_3 = \left(B\sin\left(l\,L_2\right) + A\sin mL_1\cos\left(l\,L_2\right)\right)\exp(-\beta L_2 - k\left(x - L_2\right)), \quad L_2 \le x < \infty.
\end{aligned} \tag{4.2}$$

Note that in the article [10] in the last formula there is a typo, which is corrected here. Further, due to the attenuation of the decision in the open part of the ocean, in formula (3.8) the wavenumber $k$ is taken positive $k > 0$, and the frequency $\omega$ can take both positive and negative values (in the monograph [6] $\omega > 0$, but $k$ can be both positive and negative).

In (4.2) the parameters $m$ and $l$ are determined by the formulas:

$$m = \left(-\frac{2\alpha f\,k}{\omega} - \alpha^2 - k^2\right)^{1/2}, \tag{4.3}$$

$$l = \left(\frac{2\beta f\,k}{\omega} - \beta^2 - k^2\right)^{1/2}. \tag{4.4}$$

Substituting (4.2) in (2.8), we get a system of two homogeneous equations for $A$ and $B$. The matrix of C coefficients has the form

$$C = \begin{pmatrix} \sin\left(mL_1\right)\left[\left(k-\beta\right)\cos\left(l\,L_2\right) - l\sin\left(l\,L_2\right)\right] & \left[\left(k-\beta\right)\sin\left(l\,L_2\right) + l\cos\left(l\,L_2\right)\right] \\ \sin\left(mL_1\right)\left\{\alpha+\beta\right\} + m\cos\left(mL_1\right) & -l \end{pmatrix}. \tag{4.5}$$

Equating the determinants of the matrix to zero, [10] obtained the following equation:

$$\left(\alpha + \beta + m\cot m\,L_1\right)\left[l + \left(k-\beta\right)\tan l\,L_2\right] + l\left(k - \beta - l\tan l\,L_2\right) = 0. \tag{4.6}$$

Note that [10], as well as subsequently [6], call this equation a dispersion relation. Note that in formula (4.6) we corrected another typo in the last term of work [10].

Next, when moving from (4.5) to (4.6), authors [10] make an implicit assumption: $\sin(mL_1) \neq 0$, $\cos(lL_2) \neq \neq 0$. Thus, constructed localized solutions in work [10] exist, but do not exhaust all possible scenarios.

The numerical analysis of the relation (4.6) performed [10] is as follows: the complete spectral problem allows two partial approximate solutions. The first solution is shelf waves; the solution is oscillatory in the area of the shelf and the inside of the trench and decays in the rest of the physical space. The second solution is trench waves; the solution oscillates only in the area of the marine part of the trench, fading on the shelf and in the open ocean. The authors argue that these particular solutions (shelf waves and trench waves) can be obtained as limit transitions from a common trench model; they are localized in separate parts of the trench and are solutions to the common ocean trench model with very good accuracy.

The description of these private solutions is below.

### 5. Asymptotic of the trench waves on the shelf. Crosslinking with shelf wave

The main types of bottom relief, which determine the types of trapped waves, are shown in Figure 4. In all cases, waves propagate so that in the northern hemisphere (in the southern — on the contrary) shallow water (shore) remains on the right side relative to the direction of movement.

Let's start our consideration with a solution for the littoral zone. Suppose that on the shelf the solution is oscillating. Then the wavenumber $m$, given by the relation (4.3) must be positive. For this purpose, $\omega < 0$ the condition must be met

$$\frac{-2\alpha\,k}{\alpha^2 + k^2} < \frac{\omega}{f} < 0. \tag{5.1}$$

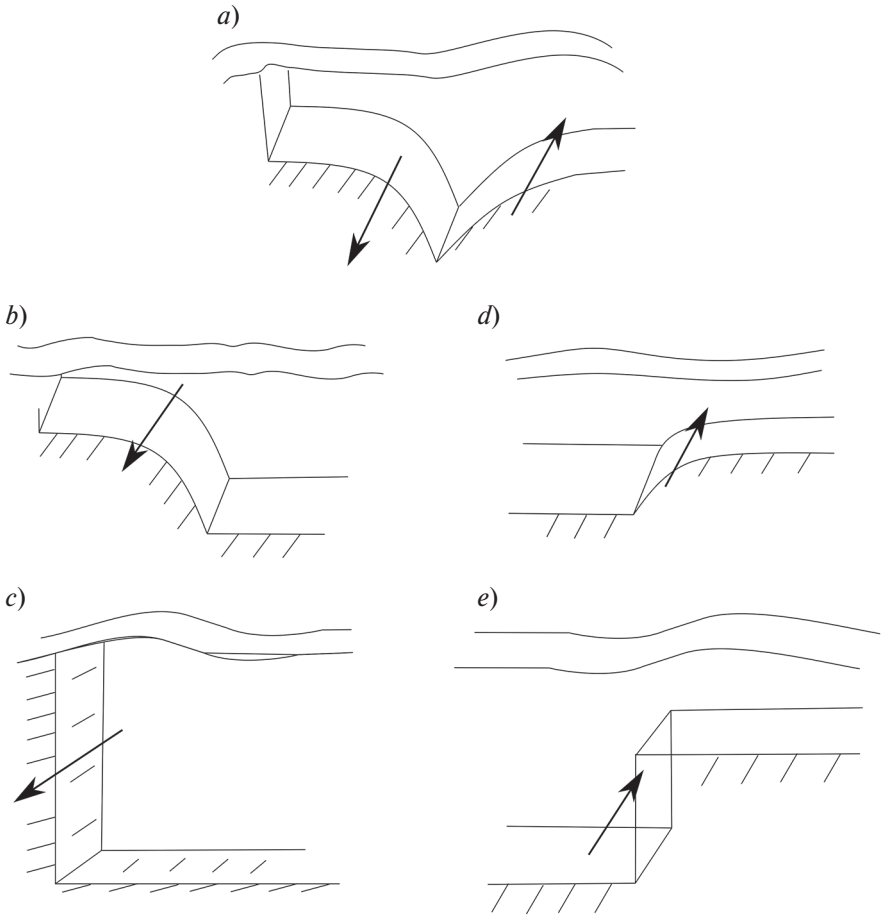


**Fig. 4**. Types of captured waves (direction shown by arrows) depending on the shape of the bottom relief: *a* — trench waves; *b* — shelf waves; *c* — Kelvin waves; *d* — internal shelf waves; *e* — Kelvin double waves

Since the y-axis is directed north, we obtain from the expression for phase in (2.5) in the longitudinal direction of the trench, we receive $\frac{\omega}{k} < 0$ . Therefore, the shelf wave phase propagates in a negative direction, i. e. to the southwest, along the shore on the right (northern hemisphere). In this case, from the relation (4.4), it is automatically obtained that the wave number $l$ in the trench part will be purely imaginary, therefore, for the trench, the solution is damped.

The first qualitative solution for the shelf is oscillation-attenuation-attenuation (direction from the shore towards the open ocean). Authors [10] crosslinked the solution as follows: from (4.6) at the limit transition $L_2 \to 0$ ($\beta$ and $l$ are limited) we get the equation

$$\left(k + \alpha\right)\sin m\, L_1 + m\cos m\, L_1 = 0 \tag{5.2}$$

or

$$\tan mL_1 = -\frac{m}{k+\alpha}, \quad m = m_n(k), \quad n = 1, 2, \ldots \tag{5.3}$$

The ratio for shelf wave amplitudes $B/A \to 0$. Such a method of sewing, in which the width of the trench part tends to zero, gives the correct result due to the fact that on the right there is a semi-infinite ocean of finite depth. However, an attempt to do the same symmetrically for the shelf part, rushing the shelf width to zero, leads to an unexpected result with a singularity. Mysak et al. [10] did not comment on this singularity and left the question open. Therefore, for the symmetry of the limit transitions of the shelf and trench waves, we make an alternative limit transition at. $L_2 \to \infty$, $\beta \to 0$. At the same time, it turns out $l \to ik$, and taking advantage

of the ratio $\tan i\, l\, L_2 = i \tanh l\, L_2$, we as a result again get the ratio (5.3). This result is extremely stable at $L_2 \to \infty$, $\beta \to 0$, does not depend on the value of the quantity $\beta L_2$, which can be either infinitely large or infinitely small. Graphical analysis of equation (5.3) is performed in the work [16], and here we will not give it.

From the side of analytics, the main idea of this part of our work is to consider trench waves as some subspecies of classical Rossby topographic waves with a classical dispersion relation. We also believe that there is no great need to introduce new classes of waves with transcendental dispersion relations. Developing this direction, we offer an alternative interpretation to approaches [10] and [6]. We believe that equations (4.3) and (4.4) are more correctly called dispersion relations for topographic waves, and we consider the ratio (4.6) and its special cases as an additional condition that determines the transverse component of the wave number.

Thus, we get some subclasses of classical topographic Rossby waves with a dispersion relation in which there is a feature in finding the transverse component of the wave number. In fact, we propose to return to the interpretation that was proposed in the first original work on this topic i.e. [16].

***Shelf waves in an alternative presentation***

Let's give a simpler interpretation of the shelf part of the solution [10] — the shelf wave in terms of topographic Rossby waves. Recall that we are talking only about sub-inertial fluctuations.

Consider formula (4.1) in relation to the shelf part of the topography. Assume $1/L = -2\alpha$, $k_1 = m$, $k_2 = k$, and substitute it in (2.12). Finally, we obtain the relation (4.3) for shelf waves in the classical form of topographic Rossby waves in the form:

$$\omega = \frac{-2\alpha f\ k}{k^2 + m^2 + \alpha^2}. \tag{5.4}$$

It is this ratio that is more correctly called the dispersion relation for shelf waves. Further, it is necessary to impose the condition that the shelf is not infinite but has a finite width $L_1$. It is geometrically clear that then a certain condition will appear that will allow us to sew the sine on the shelf side of the trench with an exponent on the ocean part of the trench for each fixed value of the wavenumber $k$, where $0 < k < \infty$ (according to [10], $k$ is considered positive). To do this, you need to find the value of $m$, by solving equation (5.3), and then get a functional connection $m = m(k)$. There will be a number of such solutions $m = m_n(k)$, $n = 1, 2, \ldots$. Next, we substitute the values found in (5.4) and plot (we apply one point on the dispersion curve). Then we take a new value of the wavenumber $k$ and repeat the procedure. Therefore, the dispersion relation for shelf waves should be recorded as

$$\omega = \frac{-2\alpha f\ k}{k^2 + m_n^2(k) + \alpha^2}, \quad n = 1, 2,. \tag{5.5}$$

Based on the result of the work [16], we will give an assessment for $m_n(k)$:

$$\frac{(n - 1/2)\pi}{L_1} < m_n(0) \le m_n(k) \le \frac{n\pi}{L_1}. \tag{5.6}$$

Functional connection $m = m(k)$ extremely low changes the dispersion curve of topographic Rossby waves. Note that [10] and [16] did not consider one special case, which should also be implemented. The condition $\sin(mL_1) = 0$ is equivalent to setting an additional solid wall at $x = 0$: $\Psi_1(0) = \Psi_2(0) = 0$. For the shelf zone, the wave number m ceases to depend on the longitudinal component of the wave vector k, so we immediately find a discrete spectrum in an explicit form:

$$\sin(mL_1) = 0, \quad m = \frac{n\pi}{L_1}, \quad n = 1, 2,\ldots \tag{5.7}$$

The wave number $l$ in the trench part is again purely imaginary, i.e. attenuation outside the shelf occurs. The dispersion relation (4.3) takes the form:

$$\omega = -\frac{2\alpha f\ k}{k^2 + m^2 + \alpha^2} = -\frac{2\alpha f\ k}{k^2 + (n\pi / L_1)^2 + \alpha^2}. \tag{5.8}$$

This relation is qualitatively similar to (5.5), but it is simpler in the sense that it does not contain an unknown dependence $m = m(k)$ and thus does not require any numerical counting. This dispersion relation is of a particular nature, but in practice, it can be useful due to its simple form and quite understandable geometric meaning: $n$ is the number of sine half-periods that fit into the shelf zone.

Next, following [16], we find the long-wave asymptotic $k \to \infty$ of the dispersion relation (5.5):

$$\omega \approx \frac{-2\alpha f\ k}{m_n^2(0) + \alpha^2}, \quad n = 1, 2, \ldots \tag{5.9}$$

The dependence on the wave number turned out to be linear, as it should be in the long-wave limit. Then the phase velocity is equal to the group velocity and equal to

$$c = c_{gr} \approx \frac{-2\alpha f}{m_n^2(0) + \alpha^2}, \quad n = 1, 2, \ldots \tag{5.10}$$

Let's move on to dimensionless variables, taking the scale of length $L_1$ is the width of the shelf part of the trench: parameter $\alpha^* = \alpha L_1$, the longitudinal wave number $k^* = kL_1$, the transverse wave number $m^* = mL_1$. Next, for ease of recording, omit the asterisks of the variables. Then the estimate of, for example, the first transverse wavenumber (the first mode) has the form:

$$\frac{\pi}{2} < m_1 \le \pi, \tag{5.11}$$

The second mode

$$\frac{3\pi}{2} < m_2 \le 2\pi. \tag{5.12}$$

For the Kuril profile, the dispersion curves of shelf and trench waves are presented in Figure 5.

## 6. Features of trench waves

Let's pay attention to the next point related to terminology. The monograph [6] (p. 102) states the following: [10] considered "Kelvin double waves propagating along the ocean side of the trench to the northeast". However, the term "Kelvin double waves" is not found at all in [10], and the authors call the solutions obtained for the "trench waves". We also adhere to the term "trench waves" [20, 21]. The term "Kelvin double waves" was introduced by Longuet-Higgins [13, 14], as the limit transition of the 0-mode on a continuous topographic feature to a topographic profile of the "step" type when the width of the topographic feature

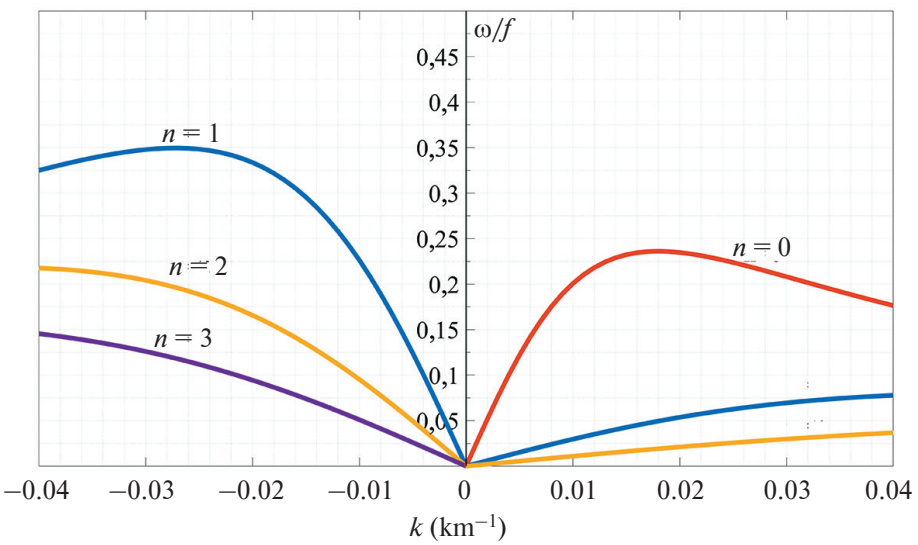


**Fig. 5**. Dispersion diagram calculated using the formula (5.8) for the Kuril region: shelf (left) and trench (right) waves

tends to zero. The maximum transition made below in our work shows the validity of the use of this term. Indeed, let the solution be oscillating in the trench, i.e. the wavenumber $l$ is real. Then it follows from (4.4) that the relation:

$$0 < \frac{\omega}{f} < \frac{2\beta k}{\beta^2 + k^2}. \tag{6.1}$$

In this case, the wavenumber $m$ automatically becomes purely imaginary $m = iM$, where $M = \left( \frac{2\alpha f k}{\omega} + \alpha^2 + k^2 \right)^{1/2}$ (a positive root sign is taken). The dispersion relation in the limit $L_1 \to 0$ ($\alpha$ — limited) has the form:

$$(k - \beta)\sin(l L_2) + l\cos(l L_2) = 0 \tag{6.2}$$

or (see [10])

$$\tan(l L_2) = -\frac{l}{k - \beta}. \tag{6.3}$$

Also, at $k = \beta$ [10] $l = 0$ — a trivial solution is believed. However, from (6.2) it is clear that there is also a non-trivial solution $\cos(lL_2) = 0$. Then the amplitude ratio for the trench waves is inverted and becomes $A/B = 0$.

***Trench waves in alternative presentment***

Let's make the following transformations: in the second formula (4.1) we assume $1/L = 2\beta$, $k_1 = l$, $k_2 = k$, and then substitute it in (2.12). Then, for the exponential topography profile, consider the dispersion relation for topographic waves

$$\omega = \frac{2\beta f k}{k^2 + l^2 + \beta^2}. \tag{6.4}$$

But (6.4) is also a dispersion relation for trench waves. Next, for each fixed value of the wavenumber $k > 0$, you need to find the value of $l$, by solving equation (6.2). Thus, we get a dependence $l = l(k)$. There will be a countable set of such solutions $l = l_n(k)$, $n = 1, 2, \ldots$, so the dispersion relation for trench waves is more correct to write in the form

$$\omega_n = \frac{2\beta f k}{k^2 + l_n^2(k) + \beta^2}, \quad n = 1, 2, \ldots \tag{6.5}$$

Further, for numerical counting, we will again move on to dimensionless variables, only taking as the length scale the width of the oceanic part of the trench $L_2$: $l^* = lL_2$, $k^* = kL_2$, $\beta^* = \beta L_2$. For the Kuril trench, we get $\beta^* = 0{,}2332$. As before, we omit asterisks for variables. Then the equation (6.3) for finding the dependence in dimensionless form for the Kuril trench takes the form

$$\tan l = -\frac{l}{k - 0.2332}. \tag{6.6}$$

This wavenumber $l$ has already been discussed above, and since it gives a very large wavelength, it is not of practical interest.

For trench waves in the Kuril trench, an important role has the presence of an open ocean of constant depth on the outside of the trench. According to the results of the work [15], which is also confirmed by the results [16], the open ocean has little effect on short trench waves, while long waves most likely become unstable. Perhaps it is this instability that gives rise to the vortex formations observed in the Kuril trench [22–27].

The limit transition $L_1 \to 0$ for the trench wave, made by the authors [10], physically means the transfer of the solid wall from the shelf to the deepest part of the trench. It is not clear how to avoid the singularity for the resulting asymptotics. It also looks somewhat strange from a physical point of view, since a limit transition is made for the shelf wave $L_2 \to \infty$, and the ocean (right) boundary of the trench is moved to infinity. At the same time, for the shelf part of the solution, the expected result is obtained, and the shelf asymptotic enters the shelf wave.

Now let's consider an alternative transition for trench asymptotics. Instead $L_1 \to 0$ let's assume, on the contrary: $L_1 \to \infty$, we move the shelf (left) border of the trench to infinity. In this case, we also add a new condition $\alpha \to 0$, the steepness of the topography tends to zero. Then the component of the wavenumber $m$ becomes purely imaginary. For certainty, assume $m = ik$, $k > 0$. Then, taking into account $\cot ik = -i\coth k$, the relation (4.6) for determining the transverse component of the wavenumber $l$ takes the form:

$$\tan l\, L_2 = \frac{2l\,k}{l^2 + \beta^2 - k^2}. \tag{6.7}$$

And this is a familiar equation for internal shelf waves, obtained [16]. Thus, we get a completely understandable physical result: in the same way as the shelf asymptotic [10] gives the shelf wave [16], the trench, the oceanic part of the solution of the trench goes to the internal shelf wave [16]. It is unclear why Mysak et al. [10] did not show this moment; it may not have worked out because they shifted the hard wall to the center of the trench.

### 7. Kelvin double wave

The classical interpretation of Kelvin double waves is based on a stepped model of topography [9]:

$$\begin{aligned} H &= H_1, \quad x < 0, \\ H &= H_2, \quad x > 0. \end{aligned} \tag{7.1}$$

In this case, equation (2.6) will take the form

$$\Psi_{xx} - k^2\Psi = 0\,. \tag{7.2}$$

The solution satisfying the attenuation at infinity has a simple form:

$$\begin{aligned} \Psi &= A\exp\left(|k|\,x\right), \quad x < 0, \\ \Psi &= A\exp\left(-|k|\,x\right), \quad x > 0. \end{aligned} \tag{7.3}$$

The wave amplitude in this case decays exponentially at the same rate on both sides of the break.

Using the sewing condition, the following dispersion relation is obtained:

$$\frac{\omega}{f} = \frac{H_2 - H_1}{H_2 + H_1}\operatorname{sgn}|k|, \tag{7.4}$$

where $H_2 > H_1$, and sgn is the sign change function. Then for a profile of the "step" type, it turns out that for any wave number, there is only one solution i. e. one subinertial mode. Note that the group velocity of these waves is always zero.

Although the term "Kelvin double wave" belongs to Longuet-Higgins [13, 14], the dispersion relation itself (7.4) seems to have been known even earlier and is also given in the work [16]. Later, Longuet-Higgins [13] considered the problem with continuous topography profiles and, using the limit transition from a continuous profile to a "step" profile, derived the second dispersion equation for Kelvin double waves. At the same time, it turned out that for a continuous profile, there is an enumerable setup of its eigenfunctions, but at the limit transition to the "step" profile, only one lower mode is insensitive to the profile shape in depth. Higher modes depend on the details of the profile and at the limit transition tend to stationary currents, on the basis of which Longuet-Higgins [13] concluded that the lowest mode is most likely to be observed in the real ocean.

A fundamentally important point is that in the next article, Longuet-Higgins [14] abandoned the dispersion relation (7.4). The reason is understandable: indeed, from a physical point of view, it is wrong if the phase velocities of long waves take infinitely large values. Longuet-Higgins [14], using more accurate (up to the second order) asymptotic decompositions, obtained that for the lower Rossby long wave mode, it is quite justified that the frequency tends to zero, and not to a constant when considering wave divergence. Essentially, for the barotropic mode, he added Rossby's barotropic radius to the denominator Россби $f^2/gH$. However, in the case where the depth profile $h(x)$ in the transition zone is exponential, this is already in contradiction with the result of Buchwald and Adams [16]. According to Longuet-Higgins [14], this contradiction is due to the fact that he took into account the horizontal divergence of wave motion. Note that these facts are not reflected in the works [6, 10, 11], although the dispersion curves constructed on the basis of numerical evaluation in the monograph

[6] correspond to the results of the Longuet-Higgins article [14]. One of these results is that the frequency tends to zero in the long wave limit. It should be noted that the limit transition procedure itself is not entirely unambiguous. The curvature of the dispersion curve for the 0-mode of a Kelvin double wave is extremely complex in the vicinity of zero (for long waves). Buchwald and Adams also note this [16]. Our estimates for the Kamchatka trench give too small wave number values, i. e. the corresponding wavelengths are most likely purely theoretical in nature since they actually go beyond the scale limits of the *f*-plane model.

In the second article of Longuet-Higgins [14], the author corrected his previous result, but it is not said in the monograph [9]. The main result is as follows: for all modes, including the lower mode (this is important), provided that wave divergence is taken into account, the group velocity of topographic Rossby waves and their phase velocity coincide in direction for long waves (with small wave numbers) and have opposite directions for short waves.

## 8. Conclusion

The following main conclusions can be drawn from the exponential topographic model of the trench. The phase of linear topographic low-frequency waves always propagates, leaving shallow water (or shore) on the right. Further, two separate classes of localized solutions can be built: one offshore, the second, in fact, also offshore, but which is usually called trench waves (in some sources this decision is mistakenly called Kelvin double waves). On the dispersion curves of both types of waves, there are both extremes (zero group velocity) and inflection points (group velocity extremum). This indicates that energy (vortices) can propagate along the shelf, both, for example, for the Kuril shelf, to the southwest (longer waves), and the northeast (shorter waves).

However, for the ocean part of the trench (for trench waves), this is not the case. Longer waves have a predominantly northeast direction of energy propagation, and shorter waves have a southwest direction. Trench waves are an order of magnitude slower (periods longer and speeds smaller) than shelf waves. This is qualitatively explained by the direct proportionality of the phase velocity of the slope of the exponential topography profile [4, 5].

Analytical models and numerical counting show that trench waves fade rather quickly toward the shelf and do not actually have a significant effect on the shelf part of the solution. Trench waves cannot be recorded while on shore, and when analyzing purely offshore solutions, it is possible not to take into account possible oscillation solutions localized on the trench.

Conversely, the shelf wave decays extremely slowly towards the trench (at least for the first mod numbers), which is extremely negative for trench localized solutions. We cannot say unequivocally that the shelf does not affect trench waves. Obviously, the effect of the shelf on the solutions localized at the trench can be manifested in a non-linear case.

The possibility of propagating topographic-type low-frequency Rossby waves captured by the Kurilo-Kamchatka trench to the pole was theoretically predicted in the studies [10, 26], which used the term "Kelvin double waves". These quasi-geostrophic waves arise due to the persistence of potential vorticity and recovery mechanisms provided by the Coriolis force and the change in ocean depth.

The analytical novelty of this work is that we managed to cross-link the trench waves [10] and the shelf waves [16], physically justified and quite expected. To do this, we proposed to infinitely increase (expand) the corresponding areas of the shelf or trench while simultaneously striving to the steepness of the topography to zero.

## Funding

The publication was made with the financial support of the St Petersburg State University Grant No. 93016972, RSF Grant No. 22-27-00004, and State assignment theme No. 0128-2021-0003.

## References

1. *Drivdal M.*, *Weber J.E.H.*, *Debernard J.B.* Dispersion relation for continental shelf waves when the shallow shelf part has an arbitrary width: Application to the shelf west of Norway. *Journal of Physical Oceanography*. 2016, 46, 2, 537–549. doi:10.1175/jpo-d-15-0023.1
2. *Gnevyshev V.G.*, *Frolova A.V.*, *Koldunov A.V.*, *Belonenko T.V.* Topographic effect for Rossby waves on a zonal shear flow. *Fundamental and Applied Hydrophysics*. 2021, 14, 1, 4–14. doi:10.7868/S2073667321010019

3. *Pedlosky J.* Geophysical fluid dynamics. *Berlin*, *Springer*, 1979. 624 p.
4. *Gnevyshev V.V.*, *Frolova A.V.*, *Belonenko T.V.* Topographic effect for Rossby waves on non-zonal shear flow. *Water Resources*. 2022, 49, 2, 240–248. doi:10.1134/S0097807822020063
5. *Gnevyshev V.G., Frolova A.V., Kubryakov A.A., Sobko Yu.V., Belonenko T.V.* Interaction between Rossby waves and a jet flow: Basic equations and verification for the Antarctic circumpolar current. *Izvestiya*, *Atmospheric and Oceanic Physics*. 2019, 55(5), 412–422. doi:10.1134/S0001433819050074
6. *Efimov V.V.*, *Kulikov E.A.*, *Rabinovich A.B.*, *Fine I.V.* Waves in the ocean boundary regions. *Leningrad*, 1985, 250 p. (in Russian).
7. *Belonenko T.V.*, *Frolova A.V.* Antarctic circumpolar current as a waveguide for Rossby waves and mesoscale eddies. *Sovremennye Problemy Distantsionnogo Zondirovaniya Zemli iz Kosmosa*. 2019, 16, 1, 181–190. doi:10.21046/2070-7401-2019-16-1-181-190 (in Russian).
8. *Belonenko T.*, *Frolova A.*, *Gnevyshev V.* Detection of waveguide for Rossby waves using satellite altimetry in the Antarctic Circumpolar Current. *International Journal of Remote Sensing*. 2020, 41:16, 6232–6247, doi:10.1080/01431161.2020.1752955
9. *LeBlond P.*, *Mysak L.A.* Waves in the Ocean. *Elsevier Scientific Publishing Company*, 1977. 602 p.
10. *Mysak L.A.*, *Leblond P.H.*, *Emery W.J.* Trench Waves. *Journal of Physical Oceanography*. 1979, 9(5), 1001–1013. doi:10.1175/1520–0485(1979)009<1001: TW>2.0.CO;2
11. *Mysak L.A.* Recent advances in shelf wave dynamics. *Reviews of Geophysics and Space Physics.* 1980, 18, 1, 211–241.
12. *Sandalyuk N.V.*, *Gnevyshev V.G.*, *Belonenko T.V.*, *Kochnev A.V.* Application of the vortex layer problem to the Gulf Stream area. *Sovremennye Problemy Distantsionnogo Zondirovaniya Zemli iz Kosmosa*. 2021, 18, 5, 242–251. doi:10.21046/2070-7401-2021-18-5-242-251 (in Russian).
13. *Longuet-Higgins M.S.* On the trapping of waves along a discontiunity of depth in a rotating ocean. *Journal of Fluid Mechanics*. 1968, 31, 3, 417–434.
14. *Longuet-Higgins M.S.* Double Kelvin waves with continuous depth profiles. *Journal of Fluid Mechanics.* 1968, 34(01), 49. doi:10.1017/s002211206800176x
15. *Mysak L.A.*, *Johnson E.R.*, *Hsiem W.W.* Baroclinic and barotropic instabilities of coastal currents. *Journal of Physical Oceanography*. 1981, 11(2), 209–230. doi:10.1175/1520–0485(1981)011<020
16. *Buchwald V.T.*, *Adams J.K.* The propagation of continental shelf waves. *Proceedings of the Royal Society A: Mathematical, Physical and Engineering Sciences*. 1968. 305(1481), 235–250. doi:10.1098/rspa.1968.0115
17. *Pelinovsky E.N.* Hydrodynamics of tsunami waves. *Nizhny Novgorod*. *IAP RAS*. 1996, 156 p. (in Russian).
18. *Didenkulova I.*, *Pelinovsky E.* On shallow water rogue wave formation in strongly inhomogeneous channels. *Journal of Physics A: Mathematical and Theoretical.* 2016, 49(19), 194001. doi:10.1088/1751-8113/49/19/194001
19. *Ermakov A.M.*, *Stepanyants Y.A.* Transformation of long surface and tsunami-like waves in the ocean with a variable bathymetry. *Pure and Applied Geophysics*. 2019, 177(3), 1675–1693. doi:10.1007/s00024-019-02259-4
20. *Rabinovich A.B.*, *Thomson R.E.* Evidence of diurnal shelf waves in satellite-tracked drifter trajectories off the Kuril Islands. *Journal of Physical Oceanography*. 2001, 31, 2650–2668. doi:10.1175/1520-0485(2001)031<2650:EODSWI>2.0.CO;2
21. *Rabinovich A.B.*, *Thomson R.E.*, *Bograd S.J.* Drifter observations of anticyclonic eddies near Bussol' Strait, the Kuril Islands. *Journal of Oceanography*. 2002, 58, 661–671. doi:10.1023/A:1022890222516
22. *Bulatov N.V.*, *Lobanov V.B.* Investigation of mesoscale eddies to the east of the Kuril Islands on the base of meteorological satellites data. *Issledovanie Zemli iz Kosmosa*. 1983, 3, 40–47 (in Russian).
23. *Rogachev K.A.* Rapid thermohaline transition in the Pacific western subarctic and Oyashio fresh core eddies. *Journal of Geophysical Research*: *Oceans*. 2000, 105, 8513–8526. doi:10.1029/1999JC900330
24. *Kaneko H.*, *Itoh S.*, *Kouketsu S.*, *Okunishi T.*, *Hosoda S.*, *Suga T.* Evolution and modulation of a poleward propagating anticyclonic eddy along the Japan and Kuril-Kamchatka trenches. *Journal of Geophysical Research*: *Oceans.* 2015, 120, 4418–4440. doi:10.1002/2014JC010693
25. *Prants S.V.*, *Lobanov V.B.*, *Budyansky M.V.*, *Uleysky M. Yu.* Lagrangian analysis of formation, structure, evolution and splitting of anticyclonic Kuril eddies. *Deep Sea Research*, *Part I.* 2016, 109, 61–75. doi:10.1016/j.dsr.2016.01.003
26. *Efimov V.V.*, *Rabinovich A.B.* On resonant tidal currents and their connection with continental shelf waves in the northwestern Pacific Ocean. *Izvestiya Akademii Nauk SSSR. Fizika Atmosfery i Okeana*. 1980, 16, 10, 1091–1101 (in Russian).
27. *Prants S.V.* Trench eddies in the Northwest Pacific: An overview. *Izvestiya*, *Atmospheric and Oceanic Physics*. 2021, 57, 4, 341–353. doi:10.1134/S0001433821040216

**Литература**

1. *Drivdal M.*, *Weber J.E.H.*, *Debernard J.B.* Dispersion relation for continental shelf waves when the shallow shelf part has an arbitrary width: Application to the shelf west of Norway // Journal of Physical Oceanography. 2016. Vol. 46, Iss. 2. P. 537–549. doi:10.1175/jpo-d-15–0023.1
2. *Гневышев В.Г., Фролова А.В., Колдунов А.В., Белоненко Т.В.* Топографический эффект для волн Россби на зональном сдвиговом потоке // Фундаментальная и прикладная гидрофизика. 2021. Т. 14, № 1. С. 4–14. doi:10.7868/S2073667321010019
3. *Pedlosky J.* Geophysical fluid dynamics. Berlin: Springer, 1979. 624 p.
4. *Gnevyshev V.V.*, *Frolova A.V.*, *Belonenko T.V.* Topographic effect for Rossby waves on non-zonal shear flow // Water Resources. 2022. Vol. 49, N 2. P. 240–248. doi:10.1134/S0097807822020063
5. *Гневышев В.Г.*, *Фролова А.В.*, *Кубряков А.А.*, *Собко Ю.В.*, *Белоненко Т.В.* Взаимодействие волн Россби со струйным потоком: основные уравнения и их верификация для Антарктического циркумполярного течения // Известия РАН. Физика атмосферы и океана. 2019. Т. 55, № 5. С. 39–50. doi:10.31857/S0002-351555539-50
6. *Ефимов В.В.*, *Куликов Е.А.*, *Рабинович А.Б.*, *Файн И.В.* Волны в пограничных областях океана. Л.: Гидрометеоиздат., 1985. 250 с.
7. *Белоненко Т.В., Фролова А.В.* Антарктическое циркумполярное течение как волновод для волн Россби и мезомасштабных вихрей // Современные проблемы дистанционного зондирования Земли из космоса. 2019. Т. 16, № 1. С. 181–190. doi:10.21046/2070-7401-2019-16-1-181-190
8. *Belonenko T.*, *Frolova A.*, *Gnevyshev V.* Detection of waveguide for Rossby waves using satellite altimetry in the Antarctic Circumpolar Current // International Journal of Remote Sensing. 2020. 41:16, P. 6232–6247, doi:10.1080/01431161.2020.1752955
9. *Ле Блон П.*, *Майсек Л.* Волны в океане, в 2-х частях / Пер. с англ. М.: Мир, 1981. 846 с.
10. *Mysak L.A.*, *Leblond P.H.*, *Emery W.J.* Trench Waves // Journal of Physical Oceanography. 1979. Vol. 9, N 5. P. 1001–1013. doi:10.1175/1520–0485(1979)009<1001: TW>2.0.CO;2
11. *Mysak L.A.* Recent advances in shelf wave dynamics // Reviews of Geophysics and Space Physics. 1980. Vol. 18, N 1. P. 211–241.
12. *Сандалюк Н.В.*, *Гневышев В.Г.*, *Белоненко Т.В.*, *Кочнев А.В.* Приложение задачи о вихревом слое для района течения Гольфстрим // Современные проблемы дистанционного зондирования Земли из космоса. 2021. Т. 18, № 5. С. 242–251. doi:10.21046/2070-7401-2021-18-5-242-251
13. *Longuet-Higgins M.S.* On the trapping of waves along a discontiunity of depth in a rotating ocean // Journal of Fluid Mechanics.1968. Vol. 31, pt. 3. P. 417–434.
14. *Longuet-Higgins M.S.* Double Kelvin waves with continuous depth profiles // Journal of Fluid Mechanics. 1968. Vol. 34, N 01. P. 49. doi:10.1017/s002211206800176x
15. *Mysak L.A.*, *Johnson E.R.*, *Hsiem W.W.* Baroclinic and barotropic instabilities of coastal currents // Journal of Physical Oceanography. 1981. Vol. 11, N 2. P. 209–230. doi:10.1175/1520–0485(1981)011<020
16. *Buchwald V.T.*, *Adams J.K.* The propagation of continental shelf waves // Proceedings of the Royal Society A: Mathematical, Physical and Engineering Sciences. 1968. Vol. 305, N 1481. P. 235–250. doi:10.1098/rspa.1968.0115
17. *Пелиновский Е.Н.* Гидродинамика волн цунами. Нижний Новгород: ИПФ РАН, 1996. 156 с.
18. *Didenkulova I.*, *Pelinovsky E.* On shallow water rogue wave formation in strongly inhomogeneous channels // Journal of Physics A: Mathematical and Theoretical. 2016. Vol. 49, N 19. P. 194001. doi:10.1088/1751-8113/49/19/194001
19. *Ermakov A.M.*, *Stepanyants Y.A.* Transformation of longsurface and tsunami-like waves in the ocean with a variable bathymetry // Pure and Applied Geophysics. 2019. Vol. 177, N 3. P. 1675–1693. doi:10.1007/s00024-019-02259-4
20. *Rabinovich A.B.*, *Thomson R.E.* Evidence of diurnal shelf waves in satellite-tracked drifter trajectories off the Kuril Islands // Journal of Physical Oceanography. 2001. Vol. 31. P. 2650–2668. doi:10.1175/1520-0485(2001)031<2650:EODSWI>2.0.CO;2
21. *Rabinovich A.B.*, *Thomson R.E.*, *Bograd S.J.* Drifter observations of anticyclonic eddies near Bussol' Strait, the Kuril Islands // Journal of Oceanography. 2002. Vol. 58. P. 661–671. doi:10.1023/A:1022890222516
22. *Булатов Н.В.*, *Лобанов В.Г.* Исследование мезомасштабных вихрей восточнее Курильских островов по данным метеорологических спутников Земли // Исследование Земли из космоса. 1983. № 3. С. 40–47.
23. *Rogachev K.A.* Rapid thermohaline transition in the Pacific western subarctic and Oyashio fresh core eddies // Journal of Geophysical Research: Oceans. 2000. Vol. 105, Iss. C4. P. 8513–8526. doi:10.1029/1999JC900330

24. *Kaneko H.*, *Itoh S.*, *Kouketsu S.*, *Okunishi T.*, *Hosoda S.*, *Suga T.* Evolution and modulation of a poleward propagating anticyclonic eddy along the Japan and Kuril-Kamchatka trenches // Journal of Geophysical Research: Oceans. 2015. Vol. 120. P. 4418–4440. doi:10.1002/2014JC010693
25. *Prants S.V.*, *Lobanov V.B.*, *Budyansky M.V.*, *Uleysky M. Yu.* Lagrangian analysis of formation, structure, evolution and splitting of anticyclonic Kuril eddies // Deep Sea Research Part I: Oceanographic Research Papers. 2016. Vol. 109. P. 61–75. doi:10.1016/j.dsr.2016.01.003
26. *Ефимов В.В.*, *Рабинович А.Б.* О резонансных приливных течениях и их связи с континентальными шельфовыми волнами в северо-западной части Тихого океана // Известия АН СССР. Физика атмосферы и океана. 1980. Т. 16, № 10. С. 1091–1101.
27. *Пранц С.В.* Вихри глубоководных желобов северо-западной части Тихого океана: обзор // Известия РАН. Физика атмосферы и океана. 2021. Т. 57, № 4. С. 387–400. doi:10.31857/S0002351521040106

## About the authors

**GNEVYSHEV Vladimir Grigoryevich**, РИНЦ Author ID: 298530, ORCID ID: 0000-0001-6654-5570, Scopus Author ID: AAZ-6352-2021, WoS ResearcherID: 6507346231, avi9783608@gmail.com

**TRAVKIN Vladimir Stanislavovich**, РИНЦ Author ID: 1023273, ORCID ID: 0000-0002-7254-9313, Scopus Author ID: 57509420800, WoS ResearcherID: HPE-4729-2023, v.travkin@spbu.ru

**BELONENKO Tatyana Vasilyevna**, РИНЦ Author ID: 66026, ORCID ID: 0000-0003-4608-7781, Scopus Author ID: 6507005889, WoS ResearcherID: K-2162-2013, btvlisab@yandex.ru

DOI:10.48612/fpg/1gan-g7mu-dk9p

УДК 535.36

© *L. S. Dolin*[1,2]*, 2023

© Translation from Russian: *E. S. Kochetkova*, 2023

[1]Institute of Applied Physics RAS, 603950, Ulyanova Str., 46, Nizhny Novgorod, Russia
[2]Lobachevsky State University of Nizhny Novgorod, 603950, Gagarin Avenue, 23, Nizhny Novgorod, Russia
*lev.dolin@ipfran.ru

# ON THE INFLUENCE OF SPATIAL FLUCTUATIONS OF THE WATER INHERENT OPTICAL PROPERTIES ON THE ENERGY OF A LIDAR ECHO SIGNAL COMING FROM A WATER

Received 08.11.2022, Revised 08.01.2023, Accepted 16.01.2023

**Abstract**

Theoretical models of the statistical characteristics of the lidar echo signal have been developed to interpret the results of optical sounding of heavily eutrophicated water bodies. Formulas are obtained for calculating the statistically average value and coefficient of variation of the energy of the elastic backscattering signal coming from the near-surface layer of water with randomly inhomogeneous absorption and scattering coefficients. Examples of the dependence of the indicated signal characteristics on the coefficients of variation of the optical characteristics of water are given. It has been established that fluctuations in the absorption coefficient lead to an increase in the average energy of the received signal, and fluctuations in the scattering coefficient to its slight decrease. A significant decrease in the average echo signal energy can be observed with cross-correlated fluctuations in the absorption and scattering coefficients, i. e. in the case when the attenuation coefficient fluctuates at a constant single scattering albedo. Considerations are made on how algorithms for estimating the average values of the optical characteristics of water and the parameters of their inhomogeneities from the average value and the coefficient of variation of the echo signal energy can be constructed.

**Keywords**: lidar, water, elastic light scattering, fluctuations in hydrooptical characteristics, statistical properties of lidar echoes

© *Л. С. Долин*[1,2]*, 2023

© Перевод с русского: *Е. С. Кочеткова*, 2023

[1]Институт прикладной физики РАН, 603950, ул. Ульянова, 46, Нижний Новгород, Россия
[2]Нижегородский государственный университет им. Н.И. Лобачевского, 603950, пр. Гагарина, 23, Нижний Новгород, Россия
*lev.dolin@ipfran.ru

# О ВЛИЯНИИ ПРОСТРАНСТВЕННЫХ ФЛУКТУАЦИЙ ГИДРООПТИЧЕСКИХ ХАРАКТЕРИСТИК НА ЭНЕРГИЮ ПРИХОДЯЩЕГО ИЗ ВОДОЕМА ЛИДАРНОГО ЭХО-СИГНАЛА

Статья поступила в редакцию 08.11.2022, после доработки 08.01.2023, принята в печать 16.01.2023

**Аннотация**

Разработаны теоретические модели статистических характеристик лидарного эхо-сигнала, предназначенные для интерпретации результатов оптического зондирования сильно эвтрофированных водоемов. Получены формулы для расчета статистически среднего значения и коэффициента вариации энергии сигнала упругого обратного рассеяния, приходящего из приповерхностного слоя воды со случайно-неоднородными показателями поглощения и рассеяния. Приведены примеры зависимости указанных характеристик сигнала от коэффициентов вариации оптических характеристик воды. Установлено, что флуктуации показателя поглощения приводят

Ссылка для цитирования: *Долин Л.С.* О влиянии пространственных флуктуаций гидрооптических характеристик на энергию приходящего из водоема лидарного эхо-сигнала // Фундаментальная и прикладная гидрофизика. 2023. Т. 16, № 1. С. 35–47. doi:10.48612/fpg/1gan-g7mu-dk9p

For citation: *Dolin L.S.* On the Influence of Spatial Fluctuations of the Water Inherent Optical Properties on the Energy of a Lidar Echo Signal Coming from a Water. *Fundamental and Applied Hydrophysics*. 2023, 16, 1, 35–47. doi:10.48612/fpg/1gan-g7mu-dk9p

к увеличению средней энергии принимаемого сигнала, а флуктуации показателя рассеяния — к ее небольшому уменьшению. Значительное уменьшение средней энергии эхо-сигнала может наблюдаться при взаимно коррелированных флуктуациях показателей поглощения и рассеяния, т. е. в случае, когда флуктуирует показатель ослабления при неизменном альбедо однократного рассеяния. Высказаны соображения о том, каким образом могут быть построены алгоритмы оценки средних значений оптических характеристик воды и параметров их неоднородностей по среднему значению и коэффициенту вариации энергии эхо-сигнала.

**Ключевые слова:** лидар, вода, упругое рассеяние света, флуктуации гидрооптических характеристик, статистические свойства лидарных эхо-сигналов

## 1. Introduction

Interpreting the results of laser sounding in oceans and freshwater bodies relies on the theory of light propagation in homogeneous or horizontally homogeneous waters, as defined by specific profiles of the water inherent optical properties (IOP) [1–26]. However, in natural conditions, the water's IOP, including the absorption and scattering coefficients, may fluctuate widely and develop randomly in time and space. Particularly large IOP fluctuations (with spatial scales of the order of a decimeter or more[1]) emerge in inland water bodies during bloom periods [27–31], and these fluctuations should be accounted for when constructing algorithms for determining the dissolved and suspended matter concentrations in water from lidar echo signals. It has been observed that a turbid layer with a given amount of absorbing substances is minimally transparent when the absorber is uniformly distributed, and fluctuations in its concentration increase the average transparency of the layer, creating a "sieve" effect [32–34]. This effect, along with the effect of shadows from IOP inhomogeneities, should manifest in the laser sounding of an aqueous medium with randomly inhomogeneous optical properties. The purpose of this work is to theoretically study the effect of the water IOP fluctuations on the characteristics of the elastic backscattering signal, namely the statistically average signal and the dispersion of its relative fluctuations. The theory presented in this paper is inspired by the theory of spatial noise arising in optical tomograms of biological tissues due to fluctuations in their optical characteristics [35–37]. The difference between the two theories stems from the fact that in tomography studies, a two-dimensional spatial signal is analyzed, while in this case, a one-dimensional signal will be examined in the form of the received light pulse energy as a function of the horizontal lidar coordinate. It happens when the lidar does not allow medium response differentiation into partial echo signals coming from different depths, for example, for waters with low transparency or when registering fluorescence signals.

## 2. Formulation of the problem

We assume that the lidar is located at a height $H$ above a flat water surface, and the radiation patterns of the emitter and receiver have a common axis oriented vertically[2]. When writing equations, we use the following notation: $W(\mathbf{r})$ is the energy of the elastic backscattering signal as a function of the coordinates of the point of intersection of the laser beam axis with the water surface $\mathbf{r}(x, y)$; $W_1$ is energy of the probing pulse; $2r_1$ and $2\vartheta_1$ are the diameter and divergence angle of the laser beam; $2r_2$ and $2\vartheta_2$ are the diameter of the entrance pupil and the angle of the field of view of the receiver; $R_F$ is Fresnel reflection coefficient of the water surface; $n_w = 1.33$ is refractive index of water; $a(\mathbf{r}, z)$, $b(\mathbf{r}, z)$ and $c(\mathbf{r}, z) = a + b$ are the water absorption, scattering and attenuation coefficients in the point $(x, y, z)$. The scattering phase function (SPF) is given as a combination of narrow $P^{\uparrow}(\theta)$ and isotropic $P^{\circ}(\theta) = 1$ SPFs with weight factors depending on the backscattering probability $p_b$:

$$P(\theta) = (1 - 2p_b)P^{\uparrow}(\theta) + 2p_b P^{\circ}(\theta), \quad p_b = (1/2)\int_{\pi/2}^{\pi} P(\theta)\sin\theta\, d\theta. \tag{1}$$

We assume that the conditions $(1/2)\int_0^{\pi} P(\theta)\sin\theta\, d\theta = 1$, $P^{\uparrow}(\theta > \pi/2) << p_b << 1$,

[1]The most rapid temporal changes in the IOP arise when the IOP inhomogeneities are transferred by currents. The characteristic time of these changes is equal to the ratio of the spatial scale of inhomogeneities to the flow velocity.
[2] In natural conditions, sounding is carried out at a certain angle to the vertical so that reflections from the water surface do not fall into the photodetector. However, this does not lead to noticeable changes in the signal coming from the water column.

$$\overline{\theta^2} = (1/2)\int_0^{\pi/2} \theta^2 P^{\uparrow}(\theta)\sin\theta\, d\theta << 1\,. \tag{2}$$

are satisfied.

The absorption and scattering coefficients are given in the form

$$a(\mathbf{r},z) = \overline{a}\left[1+\delta a(\mathbf{r},z)\right],\ b(\mathbf{r},z) = \overline{b}\left[1+\delta b(\mathbf{r},z)\right], \tag{3}$$

where $\overline{a}$ and $\overline{b}$ their statistically average values, while $\delta a$ and $\delta b$ are random relative deviations from average values. We consider fluctuations of the IOP to be spatially homogeneous and characterized by correlation functions of the form

$$B_a(\rho,\varsigma) = \overline{\delta a(\mathbf{r}+\boldsymbol{\rho}, z+\varsigma)\delta a(\mathbf{r},z)} = \overline{(\delta a)^2}\cdot R(\rho)Z(\varsigma)\ , \tag{4}$$

$$B_b(\rho,\varsigma) = \overline{\delta b(\mathbf{r}+\boldsymbol{\rho}, z+\varsigma)\delta b(\mathbf{r},z)} = \overline{(\delta b)^2}\cdot R(\rho)Z(\varsigma)\,, \tag{5}$$

$$R(\rho) = \exp\left(-\rho^2/\rho_0^2\right),\ Z(\varsigma) = ch^{-2}\left(\varsigma/\varsigma_0\right), \tag{6}$$

where $\overline{(\delta a)^2}$ and $\overline{(\delta b)^2}$ are variances of relative fluctuations of the absorption and scattering coefficients, parameters $\varsigma_0$ and $\rho_0$ are radii of vertical and horizontal correlation of fluctuations of the specified IOP. Note that the function $ch^{-2}\left(\varsigma/\varsigma_0\right)$ in (6) differs insignificantly from $\exp\left(-\varsigma^2/\varsigma_0^2\right)$, but its use instead of the Gaussian function allows one to significantly simplify the analytical expressions for the statistical characteristics of the echo signal.

### 3. Model of random realization of an echo signal

The model for the backscattered signal assumes that the horizontal correlation of IOP fluctuations has a larger radius than the horizontal size of the water volume being illuminated, and the radius of vertical correlation of these fluctuations can be of any value. Based on this assumption, the equation for the signal energy $W(\mathbf{r})$ can be derived by integrating over time the well-known expression for the power of the pulsed elastic backscattered signal coming from a water medium with horizontally homogeneous IOP, which can vary arbitrarily with depth [1, 8, 38]. This equation looks like

$$W(\mathbf{r}) = \left(\pi W_1/4\right)r_2^2\theta_2^2\int_0^{\infty} 2b_b(\mathbf{r},z)\left[\iint_{\infty} E_1\left(\mathbf{r},\mathbf{r}',z\right)E_2\left(\mathbf{r},\mathbf{r}',z\right)d^2\mathbf{r}'\right]dz\,, \tag{7}$$

$$b_b(\mathbf{r},z) = p_b b(\mathbf{r},z)\,, \tag{8}$$

where $b_b$ is backscattering coefficient, $E_1$ is irradiance at a point $(\mathbf{r}',z)$ from an auxiliary continuous source of radiation with unit power and the same parameters $2r_1$ and $2\vartheta_1$ as for a real source, while $E_2$ distribution of irradiance in water from an auxiliary continuous source with unit power, aperture diameter $2r_2$ and beam angular width $2r_2$.

The effect of a stratified aqueous medium on a laser beam structure is described with good accuracy by the radiative transfer equation in the small-angle approximation [39]. However, this solution is a Fourier integral, which complicates the calculation of the statistical moments of the signal $W$. Therefore, here we use a less accurate, but very simple, model of irradiance fields $E_{1,2}$, built based on solving the radiative transfer equation in the small-angle diffusion approximation [39]:

$$E_i\left(\mathbf{r},\mathbf{r}',z\right) = \frac{1-R_F}{\pi d_i(z)}\exp\left[-\int_0^z \alpha\left(\mathbf{r},z'\right)dz' - \left(\mathbf{r}'-\mathbf{r}\right)^2/d_i\left(z\right)\right],\ i=1,2\,, \tag{9}$$

$$\alpha\left(\mathbf{r},z\right) = a\left(\mathbf{r},z\right) + 2b_b\left(\mathbf{r},z\right), \tag{10}$$

$$d_i(z) = r_i^2 + \theta_i^2\left(H + z/n_w\right)^2 + \frac{1}{3}\overline{b}\left(1-2p_b\right)\overline{\theta^2}\cdot z^3\,. \tag{11}$$

According to the model, the distribution of irradiance in the cross-section of a light beam follows the Gaussian function, and the exponential attenuation of the total beam power α is equal to the sum of the absorption and isotropic scattering coefficients. The third term on the right side of equation (11) accounts for the effect of beam broadening due to multiple forward scattering of light. In this case, the effect of fluctuations in the scattering coefficient on the variance of the irradiance distribution $d_i$ is negligible. After substituting expressions (9)–(11) into equation (7), it takes the form

$$W(\mathbf{r}) = A\int_0^\infty 2b_b(\mathbf{r},z)\cdot\exp\left[-2\int_0^z \alpha(\mathbf{r},z')\,dz'\right]\frac{dz}{d(z)}, \tag{12}$$

$$A = \left(1-R_F\right)^2 W_1 r_2^2\theta_2^2/4\,.$$

$$d(z) = \left(r_1^2+r_2^2\right)+\left(\theta_1^2+\theta_2^2\right)\left(H+z/n_w\right)^2+\frac{2}{3}\bar{b}\left(1-2p_b\right)\overline{\theta^2}\cdot z^3\,.$$

**4. Equations for calculating the statistical characteristics of the echo signal**

Let's describe the spatial signal $W(\mathbf{r})$ by its statistical moments of the first and second order, i. e. the average value $\overline{W}$ and the correlation function

$$B_W(\rho) = \overline{W(\mathbf{r}+\boldsymbol{\rho})W(\mathbf{r})}\,, \tag{13}$$

as well as the correlation function

$$B_{\Delta W}(\rho) = \overline{\Delta W(\mathbf{r}+\boldsymbol{\rho})\Delta W(\mathbf{r})} = B_W(\rho)-\overline{W}^2 \tag{14}$$

signal fluctuation $\Delta W(\mathbf{r}) = W(\mathbf{r})-\overline{W}$, dispersion of its fluctuations

$$d_W = B_{\Delta W}(0)\,, \tag{15}$$

fluctuation spatial correlation coefficient

$$K(\rho) = B_{\Delta W}(\rho)/B_{\Delta W}(0) \tag{16}$$

and signal variation coefficient

$$\delta_W = \sqrt{d_W}/\overline{W}\,. \tag{17}$$

For a better understanding of why the fluctuations of different IOPs manifest themselves differently in the echo signal, the calculation of its statistical characteristics was performed for cases where fluctuates either one of the parameters *a* or *b*, or the attenuation coefficient $c = a + b$ while maintaining the single scattering albedo $\omega_0 = b/c$.

**A. Only the absorbance fluctuates.** Under the condition $\delta b = 0$ the equation (12) becomes

$$W(\mathbf{r}) = 2p_b\bar{b}A\int_0^\infty \exp\left[-2\Delta\tau_a\left(\mathbf{r},z\right)\right]F_a(z)dz\,, \tag{18}$$

$$\Delta\tau_a\left(\mathbf{r},z\right) = \bar{a}\int_0^z \delta a(\mathbf{r},z')\,dz'\,,\quad F_a(z) = \exp\left[-2\left(\bar{a}+2p_b\bar{b}\right)z\right]/d(z)\,. \tag{19}$$

If we assume that the exponent $\varphi = -2\Delta\tau_a\left(\mathbf{r},z\right)$ on the right side of equation (18) is normally distributed, then the statistical averaging of the function $W$ can be done using the relation

$$\overline{\exp(\varphi)} = \exp\left[\overline{\varphi^2}/2\right]. \tag{20}$$

This relation can also be used to find the function $B_W(\boldsymbol{\rho})$, assuming that $2\left[\ _a\left(\mathbf{r}\quad\boldsymbol{\rho},z_1\right)\quad\ _a\left(\mathbf{r},z_2\right)\right]$. As a result, we find:

$$\overline{W} = 2p_b\bar{b}A\int_0^\infty \exp\left[2\overline{\left(\Delta\tau_a(\mathbf{r},z)\right)^2}\right]F_a(z)dz\,, \tag{21}$$

$$B_{\Delta W}(\rho) = \left(2p_b\bar{b}A\right)^2 \int_0^\infty\int_0^\infty \left[\exp\left(4\overline{\Delta\tau_a(\mathbf{r}+\boldsymbol{\rho},z_1)\Delta\tau_a(\mathbf{r},z_2)}\right)-1\right]\times$$
$$\times\left[\exp\left(2\overline{\left(\Delta\tau_a\left(\mathbf{r},z_1\right)\right)^2}+2\overline{\left(\Delta\tau_a\left(\mathbf{r},z_2\right)\right)^2}\right)\right]F_a(z_1)F_a(z_2)dz_1dz_2, \quad (22)$$

$$\overline{\Delta\tau_a(\mathbf{r}+\boldsymbol{\rho},z_1)\Delta\tau_a(\mathbf{r},z_2)} = \overline{(\delta a)^2}\,R(\rho)\left(\bar{a}\varsigma_0\right)^2 \ln\frac{ch(z_1/\varsigma_0)ch(z_2/\varsigma_0)}{ch\left[(z_1-z_2)/\varsigma_0\right]}, \quad (23)$$

$$\overline{\left(\Delta\tau_a(\mathbf{r},z)\right)^2} = 2\overline{(\delta a)^2}\left(\bar{a}\varsigma_0\right)^2 \ln\left[ch(z/\varsigma_0)\right]. \quad (24)$$

**B. Only the scattering coefficient fluctuates.** Freezing $\delta a = 0$, equation (12) and the equations for calculating the statistical moments of the echo signal energy can be written as

$$W(\mathbf{r}) = A\int_0^\infty 2b_b\left(\mathbf{r},z\right)\exp\left(-4\int_0^z b_b(\mathbf{r},z')\,dz'\right)\frac{\exp\left(-2\bar{a}z\right)dz}{d(z)} =$$
$$= \left(A/2\right)\int_0^\infty\left\{1-\exp\left[-4p_b\left(\bar{b}z+\Delta\tau_b\left(\mathbf{r},z\right)\right)\right]\right\}F_b(z)dz, \quad (25)$$

$$\Delta\tau_b\left(\mathbf{r},z\right) = \bar{b}\int_0^z \delta b\left(\mathbf{r},z'\right)dz',\ F_b(z) = -\frac{d}{dz}\left[\frac{\exp\left(-2\bar{a}z\right)}{d(z)}\right], \quad (26)$$

$$\overline{W} = \left(A/2\right)\int_0^\infty\left\{1-\exp\left[-4p_b\bar{b}z+8p_b^2\overline{\left(\Delta\tau_b\left(\mathbf{r},z\right)\right)^2}\right]\right\}F_b(z)\,dz, \quad (27)$$

$$B_{\Delta W}(\rho) = \left(A^2/4\right)\int_0^\infty\int_0^\infty\left[\exp\left(16p_b^2\overline{\Delta\tau_b(\mathbf{r}+\boldsymbol{\rho},z_1)\Delta\tau_b(\mathbf{r},z_2)}\right)-1\right]\times$$
$$\times\left[\exp\left(-4p_b\bar{b}(z_1+z_2)+8p_b^2\overline{\left(\Delta\tau_b(\mathbf{r},z_1)\right)^2}+8p_b^2\overline{\left(\Delta\tau_b(\mathbf{r},z_2)\right)^2}\right)\right]F_b(z_1)F_b(z_2)\,dz_1\,dz_2. \quad (28)$$

Expressions for the statistical moments of the function $\Delta\tau_b\left(\mathbf{r},z\right)$ are obtained from (23) and (24) by replacing $\overline{(\delta a)^2}\to\overline{(\delta b)^2}$, $\bar{a}\to\bar{b}$.

**C. The attenuation coefficient fluctuates with the single scattering albedo unchanged.** Assuming that the condition $\omega_0 = b/c = \bar{b}/\bar{c} = \text{const}$ holds, and fluctuations of the attenuation coefficient $c = a + b$ are described by the equations

$$c(\mathbf{r},z) = \bar{c}\left[1+\delta c(\mathbf{r},z)\right], \quad (29)$$

$$B_c(\rho,\varsigma) = \overline{\delta c(\mathbf{r}+\boldsymbol{\rho},z+\varsigma)\delta c(\mathbf{r},z)} = \overline{(\delta c)^2}\cdot R(\rho)Z(\varsigma), \quad (30)$$

then equation (12) and equations for calculating the statistical moments of the echo signal energy can be written as

$$W(\mathbf{r}) = C\int_0^\infty\left\{1-\exp\left[-2k\left(\bar{c}z+\Delta\tau(\mathbf{r},z)\right)\right]\right\}F_c(z)dz, \quad (31)$$

$$k = 1-\left(1-2p_b\right)\omega_0,\ C = \omega_0 p_b A/k, \quad (32)$$

$$\Delta\tau\left(\mathbf{r},z\right) = \bar{c}\int_0^z \delta c\left(\mathbf{r},z'\right)dz',\ F_c(z) = -\frac{d}{dz}\left(d(z)\right)^{-1}, \quad (33)$$

$$\overline{W} = C\int_0^\infty\left[1-\exp\left(-2k\bar{c}z+2k^2\overline{\left(\Delta\tau(\mathbf{r},z)\right)^2}\right)\right]F_c(z)dz, \quad (34)$$

$$B_{\Delta W}(\rho) = C^2 \int_0^\infty \int_0^\infty \left[ \exp\left(4k^2 \overline{\Delta\tau(\mathbf{r}+\boldsymbol{\rho}, z_1)\Delta\tau(\mathbf{r}, z_2)}\right) - 1 \right] \times$$

$$\times \left[ \exp\left( -2k\overline{c}(z_1+z_2) + 2k^2 \overline{\left(\Delta\tau(\mathbf{r}, z_1)\right)^2} + 2k^2 \overline{\left(\Delta\tau(\mathbf{r}, z_2)\right)^2} \right) \right] F_c(z_1) F_c(z_2)\, dz_1\, dz_2 . \quad (35)$$

Expressions for the statistical moments of the function $\Delta\tau(\mathbf{r}, z)$ are obtained from (23) and (24) by replacing $\overline{(\delta a)^2} \to \overline{(\delta c)^2}$, $\overline{a} \to \overline{c}$.

### 5. Numerical analysis of the statistical characteristics of the echo-signal

As follows from equations (12)–(35), the expressions for the statistical characteristics of the echo signal can be represented as functions of a dimensionless variable $\overline{c}\rho$ and dimensionless parameters $\hat{\omega}_0 = \overline{b} / \overline{c}$, $\overline{c}\rho_0$, $\overline{c}\varsigma_0$, $\overline{(\delta a)^2}$, $\overline{(\delta b)^2}$, $\overline{(\delta c)^2}$, $\overline{c}(r_1^2 + r_2^2)^{1/2}$, $\overline{c}H$. Figures 1, *a*; 2, *a* and 3, *a* show the results of calculating the parameter

$$N = \frac{\overline{W} - W_0}{W_0}, \quad (36)$$

which characterizes the difference between the statistically average energy $\overline{W}$ of a fluctuating echo signal and the energy $W_0$ of a regular signal, generated by an aqueous medium with spatially uniform optical characteristics $a = \overline{a}$, $b = \overline{b}$. The curves of these figures depict the dependence of the parameter $N$ on the variation coefficients

$$\delta_a = \sqrt{\overline{(\delta a)^2}}, \ \delta_b = \sqrt{\overline{(\delta b)^2}} \ \ \delta_c = \sqrt{\overline{(\delta c)^2}} \quad (37)$$

of absorption coefficients, scattering and attenuation at three different values of the parameter $\hat{\omega}_0$ in $\overline{c}\varsigma_0 = 0.75$, $\overline{c}(r_1^2 + r_2^2)^{1/2} = 0.175$, $\overline{c}H = 5$ case. Figures 1, *a*; 2, *a* and 3, *a* illustrate the dependence of the coefficient of variation $\delta_W$ of the echo signal energy (equation (17)) on the value of parameters (37) and $\hat{\omega}_0$ for the above values of the other three parameters.

The figures show that the spatial fluctuations of different IOPs manifest themselves differently in the echo signal. Fluctuations in the absorption coefficient (with its fixed average value) can lead to a significant increase in the statistically averaged signal (Fig. 1, *a*), while fluctuations in the scattering coefficient reduce it, but very slightly (Fig. 2, *a*). With cross-correlated fluctuations in the absorption and scattering coefficients (i.e., fluctuations in the attenuation coefficient for a given single scattering albedo), the average signal can decrease significantly (Fig. 3, *a*).

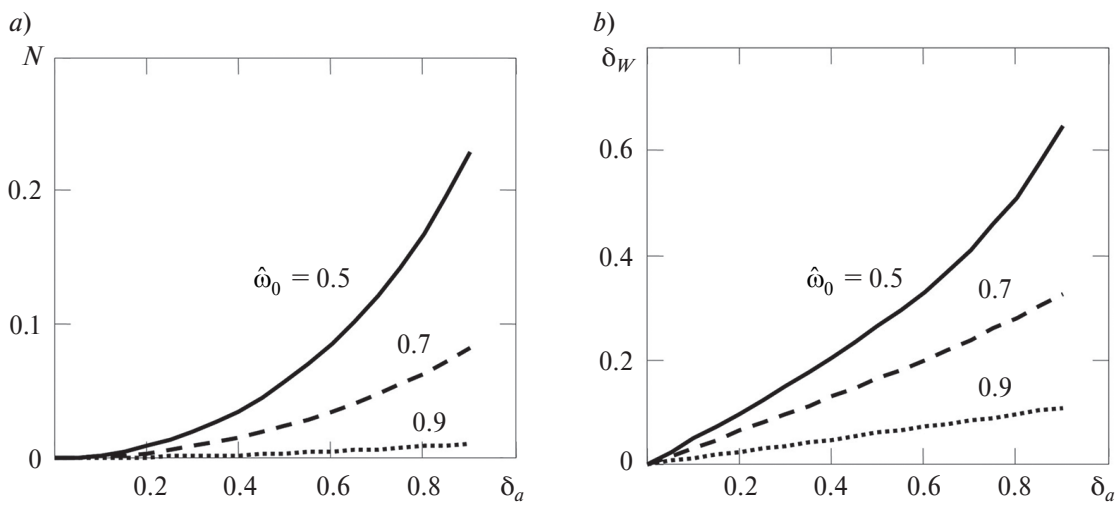


**Fig. 1**. Dependence of the parameters $N$ (*a*) and $\delta_W$ (*b*) (see eq. (36) and (17)) on the absorbance variation coefficient $\delta_a$ at the values of the parameter $\hat{\omega}_0$, indicated in the figures and assuming $\overline{c}\varsigma_0 = 0.75$, $\overline{c}(r_1^2 + r_2^2)^{1/2} = 0.175$, $\overline{c}H = 5$.

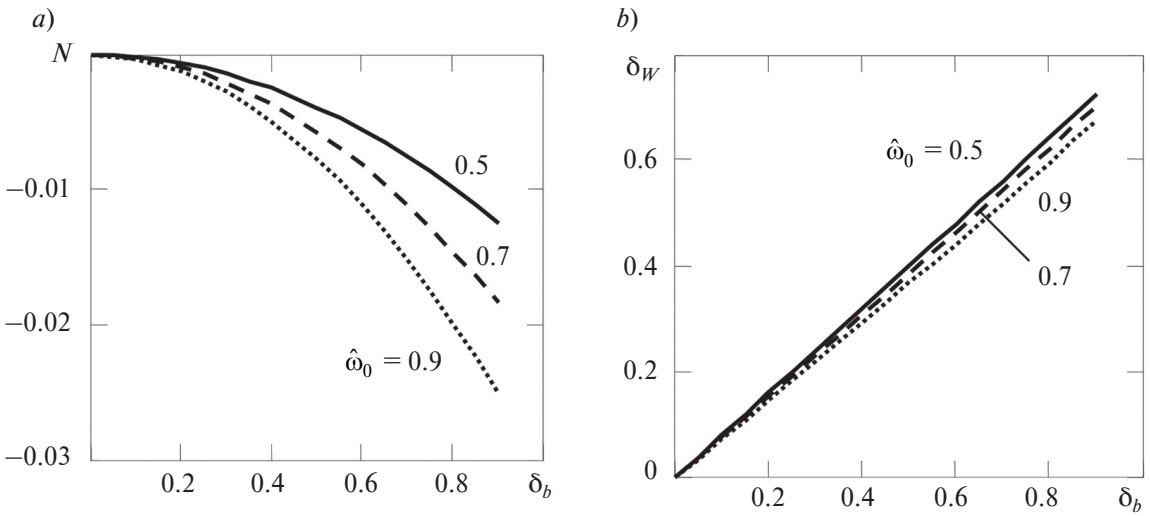


**Fig. 2**. Dependence of the parameters $N$ (*a*) and $\delta_W$ (*b*) on the variation coefficient $\delta_b$ of the scattering coefficient under the conditions indicated in the caption to Fig. 1

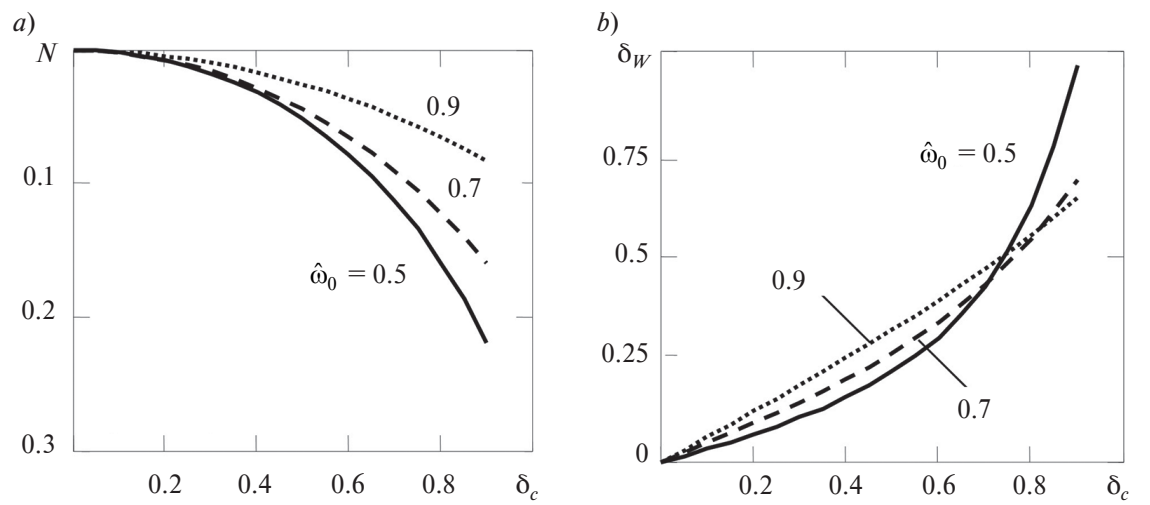


**Fig. 3**. Dependence of the parameters $N$ (*a*) and $\delta_W$ (*b*) on the on the variation coefficient $\delta_c$ of the attenuation coefficient under the conditions indicated in the caption to Fig. 1

In the three cases under consideration, the numerical values of the coefficient of variation of the signal $\delta_W$ (assuming $\delta_a = \delta_b = \delta_c$) differ (Fig. 1, *b*; Fig. 2; *b*, Fig. 3, *b*), but not as significant as the parameter $N$ values, characterizing the fluctuations' effect of the IOP on the average signal energy. The curves in Figures 1, *a* and *b*, depicting the dependence of the parameters $N$ and $\delta_W$ on the coefficient of variation of the absorption index $\delta_a$ are very similar to each other, which is not true about the corresponding curves in Figures 2 and 3. Spatial fluctuations in the scattering coefficient cause strong variations in the echo signal (Fig. 2, *b*) but do not have a significant effect on its average value. The dependence $\delta_W(\delta_c)$ at $\hat{\omega}_0 = 0.5$ (Fig. 3, *b*) is similar to the dependence $\delta_W(\delta_a)$ (Fig. 1, *b*), and at $\hat{\omega}_0 = 0.9$ it almost coincides with the dependence $\delta_W(\delta_b)$ (Fig. 2, *b*).

Note that an increase in the average energy of the echo signal due to fluctuations in the absorption coefficient is a direct manifestation of the "sieve" effect, which leads to an increase in the thickness of the water layer from which the signal comes. While the decrease is due to fluctuations in the attenuation coefficient or scattering coefficient that occurs when the upper part of each of the clot of absorbing and scattering substances obscures its lower part.

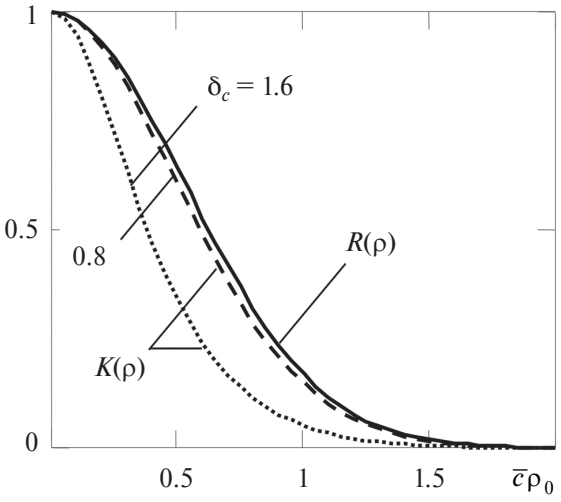


**Fig. 4**. The spatial correlation coefficient $K(\rho)$ of the echo signal fluctuations for the variation coefficient of the attenuation coefficient $\delta_c = 0.8$, 1.6; $R(\rho)$ is the horizontal correlation coefficient of attenuation coefficient fluctuation; $\bar{c}\rho_0 = 0.75$; $\omega_0 = 0.7$; $R(\rho)$ — see equation (6); other parameters are indicated in the caption to Figure 1

Figure 4 shows the calculated coefficient of spatial correlation $K(\rho)$ of echo signal energy fluctuations generated by inhomogeneities of the water attenuation coefficient (equations (16), (35)). The figure shows that in the case under consideration, the function $K(\rho)$ differs significantly from the coefficient of horizontal correlation $R(\rho)$ of the attenuation coefficient fluctuations only at very large values of its variation coefficient $\delta_c$.

### 6. A possible method for estimating the optical properties of water by the average value and the coefficient of variation of the echo signal energy

Assuming for definitiveness that the fluctuating characteristic of water is the attenuation coefficient, then the form of the functions $N$ and $\delta_W$, shown in Fig. 3 will depend on the average values $\bar{c}$, $\bar{b}$ the attenuation and scattering coefficients, the backscattering probability $p_b$, the parameter of the scattering phase function $\overline{\theta^2}$ and the vertical correlation radius $\varsigma_0$ of the attenuation coefficient fluctuations. By measuring two statistical parameters of the signal $\overline{W}$ and $\delta_W$, we can complete only two equations for solving the inverse problem, which indicates the impossibility of solving it without using some a priori information about the optical characteristics of water.

As can be seen from Fig. 4, under the condition $\delta_c < 1$ the correlation radius of fluctuations in the echo signal energy $\rho_W$ ((the function width $K(\rho)$ at the $1/e$ level) practically does not differ from the horizontal correlation radius $\rho_0$ of fluctuations of the attenuation coefficient (the function width $R(\rho)$ at the $1/e$ level). Therefore, assuming that fluctuations of the attenuation coefficient are isotropic, we can estimate the vertical radius of their correlation using relationship $\varsigma_0 = \rho_W$.

To reduce the number of unknown parameters in the echo-signal models, one could use empirical correlations between different IOPs, similar to the Levin-Kopelevich regressions [40, 41], which allow one to express the parameters $\bar{b}$, $p_b$ and $\overline{\theta^2}$ through the attenuation coefficient $\bar{c}$. These regressions were obtained for marine waters with attenuation $\bar{c} = (0.3 \div 1)$ m$^{-1}$ at a wavelength of 500 nm. The search for similar regressions for blooming inland water bodies is also underway [29]. Removing parameters $\bar{b}$, $p_b$ and $\overline{\theta^2}$ from the theoretical expressions for $\overline{W}$, $W_0$, $N$ and $\delta_W$ using empirical regressions, would allow the definition of the remaining two parameters $\bar{c}$ and $\delta_c$ using the equations

$$W_0(\bar{c})\left[1 + N(\bar{c}, \delta_c)\right] = \overline{W'}, \ \delta_W(\bar{c}, \delta_c) = \delta'_W, \tag{38}$$

where $\overline{W'}$ and $\delta'_W$ are measured values of the statistical characteristics of the signal; $W_0 = \overline{W}(\delta_c = 0)$ is the energy of the signal coming from a reservoir with uniform optical properties. After finding the parameter $\bar{c}$ the rest of the IOPs are determined using the same regressions as for equations (38).

### 7. Conclusion

The main goal of this work was to study the effect mechanisms of spatial fluctuations of various IOPs on lidar echo signals, which required the maximum simplification of the water optical properties models. However,

the proposed estimation method for the statistical characteristics of echo signals is also quite suitable for theory development for lidar sounding of natural water bodies. The study showed that fluctuations in the absorption, scattering, and attenuation coefficients (with the single scattering albedo unchanged) are approximately the same in echo signal fluctuations but produce a different effect on their average energy. Absorption coefficient fluctuations increase average energy, while fluctuations of attenuation and scattering coefficients decrease average signal energy at significantly different rates. Such manifestations of IOP fluctuations are qualitatively explained by two effects, an increase in the average transparency of the water layer due to fluctuations in the absorption coefficient ("sieve effect") and the formation of shadows behind the inhomogeneities of the attenuation coefficient, which decreases the reflectivity of the water layer. These effects should be accounted for when constructing algorithms for determining the optical characteristics of heavily eutrophicated waters from lidar signals.

Note that the water surface may have unwanted effects on the signal received by a surface lidar and requires special measures to eliminate these effects. The most obvious (but seldom available) option is to observe in calm conditions. Surface waves modulate the power and energy of the signal and become a source of multiplicative interference, which makes it difficult to measure the IOP. This interference can be addressed in a similar manner as when enhancing the visibility of underwater objects under natural light conditions in rough water [42]. The method involves removing signal distortions by utilizing information about the topography of the surface through which the scattered light enters the photodetector. This information can be obtained by analyzing images captured by a specialized video camera and processing them to determine the surface's relief [43].

**Funding**

The work was carried out as part of the implementation of the Strategic Academic Leadership Program "Priority 2030" of UNN (direction № N-468–99_2021–2023) and according to the State assignment (theme № 0030–2021–0006).

## References

1. *Dolin L.S.*, *Savel'ev V.A.* Backscattering signal characteristics at pulse narrow beam illumination of a turbid medium. *Izvestiya Academy of Science USSR*, *Atmospheric and Oceanic Physics*. 1971, 7, 5, 505–510 (in Russian).
2. *Bravo-Zhivotovsky D.M.*, *Gordeev L.B.*, *Dolin L.S.*, *Mochenev S.B.* Determining the absorption and scattering coefficients of sea water by some characteristics of a light field of artificial light sources. *Hydrophysical and hydrooptics investigations in the Atlantic and the Pacific Oceans* / Ed. By Monin A.S., Shifrin K.S. *M.*, *Nauka*, 1974, 153–158 (in Russian).
3. Ocean optics / Ed. By Monin A.S. *M.*, *Nauka*, 1983. Vol. 1. Physical optics of the ocean. 371 p. (in Russian).
4. *Billard B.*, *Abbot R.H.*, *Penny M.F.* Airborne estimation of sea turbidity parameters from the WRELANDS laser airborne depth sounder. *Applied Optics*. 1986, 25, 2080–2088.
5. *Bravo-Zhivotovsky D.M.*, *Dolin L.S.*, *Savel'ev V.A.*, *Fadeev V.V.*, *Shchegol'kov Yu.B.* Optical methods for sounding of the ocean: laser remote sensing. *Methods of Remote Sensing of the Ocean* / Ed. By Bravo-Zhivotovsky D.M., Dolin L.S. *Institute of Applied Physics*, *Gorky*, *USSR*, 1987, 84–125 (in Russian).
6. *Hoge F.E.*, *Wright C.W.*, *Krabill W.B.*, *Buntzen R.R.*, *Gilbert G.D.*, *Swift R.N.*, *Yungel J.K.*, *Berry R.E.* Airborne lidar detection of subsurface oceanic scattering layers. *Applied Optics*. 1988, 27, 3969–3977.
7. *Vasilkov A.P.*, *Kondranin T.V.*, *Myasnikov E.V.* Determination of the profile of the light scattering index from the polarization characteristics of back-reflected radiation in pulsed sounding of the ocean. *Izvestiya Academy of Science USSR*, *Atmospheric and Oceanic Physics*. 1990, 26, 3, 307–312 (in Russian).
8. *Dolin L.S.*, *Levin I.M.* Handbook on the Theory of Underwater Vision. *Leningrad*, *Gidrometeoizdat*, 1991. 230 p. (in Russian).
9. *Dolin L.S.*, *Levin I.M.* Optics, Underwater. Encyclopedia of Applied Physics. *VCH Publishers*, 1995, 12, 571–601.
10. *Vasilkov A.P.*, *Goldin Yu.A.*, *Gureev B.A.* Determination of the vertical distribution of the seawater scattering index using an aviation polarization lidar. *Izvestiya*, *Atmospheric and Oceanic Physics*. 1997, 33, 4, 563–569 (in Russian).
11. *Vasilkov A.P.*, *Goldin Y.A.*, *Gureev B.A.*, *Hoge F.E.*, *Swift R.N.*, *Wright C.W.* Airborne polarized lidar detection of scattering layers in the ocean. *Applied Optics*. 2001, 40, 24, 4353–4364. doi:10.1364/AO.40.004353
12. *Bissonnette L.R.*, *Roy G.*, *Poutier L.*, *Cober S.G.*, *Isaac G.A.* Multiple-scattering lidar retrieval method: tests on Monte Carlo simulations and comparisons with *in situ* measurements. *Applied Optics*. 2002, 41, 30, 6307–6324. doi:10.1364/AO.41.006307

13. *Feygels V.I.*, *Kopilevich Y.I.*, *Surkov A.*, *Yangel J.K.*, *Behrenfeld M.J.* Airborne lidar system with variable field-of-view receiver for water optical measurements. *Proceedings of SPIE. Ocean Remote Sensing and Imaging II*. 2003, 5155, 12–21.
14. *Kokhanenko G.P.*, *Krekova M.M.*, *Penner I.E.*, *Shamanaev V.S.* Detection of hydrosol inhomogeneities by a polarizing lidar. *Atmospheric and Oceanic Optics*. 2004, 17, 9, 750–758. (in Russian).
15. *Kopilevich Yu.*, *Feygels V.I.*, *Tuell G.H.*, *Surkov A.* Measurement of ocean water optical properties and seafloor reflectance with scanning hydrographic operational airborne lidar survey (SHOALS): I. Theoretical background. *Proceedings of SPIE*. 2005, 5885, 9 p.
16. *Tuell G.H.*, *Feygels V.*, *Kopilevich Yu.*, *Weidemann A.D.*, *Cunningham A.G.*, *Mani R.*, *Podoba V.*, *Ramnath V.*, *Park J.Y.*, *Aitken J.* Measurement of ocean water optical properties and seafloor reflectance with scanning hydrographic operational airborne lidar survey (SHOALS): II. Practical results and comparison with independent data. *Proceedings of SPIE*. 2005, 5885, 13 p.
17. *Hoge F.E.* Oceanic inherent optical properties: proposed single laser lidar and retrieval theory. *Applied Optics*. 2005, 44, 34, 7483–7486. doi:10.1364/AO.44.007483
18. *Churnside J.H.*, *Thorne R.E.* Comparison of airborne lidar measurements with 420 kHz echo-sounder measurements of zooplankton. *Applied Optics*. 2005, 44, 26, 5504–5514. doi:10.1364/AO.44.005504
19. *Zege E.*, *Katsev I.*, *Prikhach A.* Retrieval of seawater inherent optical properties profiles from lidar waveforms. *Proceedings of SPIE*. 2007, 6615, 66150B, 10 p.
20. *Dolina I.S.*, *Dolin L.S.*, *Levin I.M.*, *Rodionov A.A.*, *Savel'ev V.A.* Inverse problems of lidar sensing of the ocean In: Current Research on Remote Sensing, Laser Probing, and Imagery in Natural Waters. *Proceeding of SPIE*. 2007, 6615, 66150C — 1–10.
21. *Dolin L.S.* Lidar method for measurement of the modulation transfer function of water layers. *Fundamental and Applied Hydrophysics*. 2010, 3(9), 62–71 (in Russian).
22. *Kokhanenko G.P.*, *Balin Yu.S.*, *Penner I.E.*, *Shamanaev V.S.* Lidar and in situ measurements of optical parameters of water surface layers in Lake Baikal. *Atmospheric and Oceanic Optics*. 2011, 24, 478–486. doi:10.1134/S1024856011050083
23. *Palmer S.C.J.*, *Pelevin V.V.*, *Goncharenko I.*, *Kovács A.W.*, *Zlinszky A.*, *Présing M.*, *Horváth H.*, *Nicolás-Perea V.*, *Balzter H.*, *Tóth V.R.* Ultraviolet fluorescence LiDAR (UFL) as a measurement tool for water quality parameters in turbid lake conditions. *Remote Sensing*. 2013, 5, 4405–4422. doi:10.3390/rs5094405
24. *Pelevin V.*, *Zavialov P.*, *Konovalov B.*, *Abramov O.*, *Grabovskiy A.*, *Goncharenko I.* Remote Laser Sensing of the Seas and Inland Waters Bodies using Portable Fluorescent Lidars(UFL series). *Proceedings of VIII International Conference* "*Current problems in optics of natural waters*" (ONW'2015). *St. Petersburg*, 2015, 179–184 (in Russian).
25. *Glukhov V.A.*, *Goldin Yu.A.*, *Rodionov M.A.* Experimental estimation of the capabilities of the lidar PLD-1 for the registration of various hydro-optical irregularities of the sea water column. *Fundamental and Applied Hydrophysics*. 2017, 10, 2, 41–48. doi:10.7868/S207366731702006X (in Russian).
26. *Glukhov V.A., Goldin Yu.A., Rodionov M.A.* Method of Internal Waves Registration by Lidar Sounding in Case of Waters with Two-Layer Sratification of Hydrooptical Characteristics. *Fundamental and Applied Hydrophysics*. 2021, 14, 3, 86–97. doi:10.7868/S2073667321030084 (in Russian).
27. *Lednev V.N.*, *Grishin M. Ya.*, *Pershin S.M.*, *Bunkin A.F.*, *Kapustin I.A.*, *Molkov A.A.*, *Ermakov S.A.* Laser remote probing of freshwater reservoir with high phytoplankton concentration. *Sovremennye Problemy Distantsionnogo Zondirovaniya Zemli iz Kosmosa*. 2016, 13, 1, 119–134 (in Russian). doi:10.21046/2070-7401-2016-13-1-119-134
28. *Grishin M. Ya.*, *Lednev V.N.*, *Pershin S.M.*, *Bunkin A.F.*, *Kobylyanskiy V.V.*, *Ermakov S.A.*, *Kapustin I.A.*, *Molkov A.A.* Laser remote sensing of an algal bloom in a freshwater reservoir. *Laser Physics*. 2016, 26, 125601 (8pp). doi:10.1088/1054–660X/26/12/125601
29. *Molkov A.A.*, *Kapustin I.A.*, *Shchegolkov Yu.B.*, *Vodeneeva E.L.*, *Kalashnikov I.N.* On correlation between inherent optical properties at 650 nm, Secchi depth and blue-green algal abundance for the Gorky reservoir. *Fundamental and Applied Hydrophysics*. 2018, 11, 3, 26–33. doi:10.7868/S2073667318030036
30. *Molkov A.A.*, *Fedorov S.V.*, *Pelevin V.V.*, *Korchemkina E.N.* On regional models for high-resolution retrieval of Chlorophyll a and TSM concentrations in the Gorky Reservoir by Sentinel-2 imagery. *Remote Sensing*. 2019, 10, 11, 1215–1241. doi:10.3390/rs11101215
31. *Molkov A.A., Pelevin V.V., Korchemkina E.N.* Approach of non-station-based in situ measurements for high resolution satellite remote sensing of productive and highly changeable inland waters. *Fundamental and Applied Hydrophysics*. 2020, 13(2), 60-67. doi:10.7868/S2073667320020070
32. *Fukshansky L.* Absorption statistics in turbid media. *Journal of Quantitative Spectroscopy and Radiative Transfer*. 1987, 38, 389–406.

33. *McClendon J.H.*, *Fukshansky L.* On the interpretation of absorption spectra of leaves — II. The non-absorbed ray of the sieve effect and the mean optical pathlength in the remainder of the leaf. *Photo-chem Photobiol.*1990, 51, 211–216.
34. *Anisimov O.*, *Fukshansky L.* Stochastic radiation in macroheterogeneous random optical media. *Journal of Quantitative Spectroscopy and Radiative Transfer*. 1992, 48, 169–186.
35. *Dolin L.S.*, *Sergeeva E.A.*, *Turchin I.V.* Shadow noise in OCT images of biological tissues. *Quantum Electronics*. 2008, 38, 6, 543–550. doi:10.1070/QE2008v038n06ABEH013839
36. *Dolin L.S.* Development of the radiative transfer theory as applied to instrumental imaging in turbid media. *Physics — Uspekhi*. 2009, 52, 5, 519–526. doi:10.3367/UFNe.0179.200905k.0553
37. *Dolin L.S.*, *Sergeeva E.A.*, *Turchin I.V.* Correlation characteristics of optical coherence tomography images of turbid media with statistically inhomogeneous optical parameters. *Journal of Quantitative Spectroscopy and Radiative Transfer*. 2012, 113, 9, 691–703. doi:10.1016/j.jqsrt.2012.02.004
38. *Dolin L.S.*, *Dolina I.S.*, *Saveliev V.A.* A lidar method for determining internal wave characteristics. *Izvestiya*, *Atmospheric and Oceanic Physics*. 2012, 48, 4, 444–453. doi:10.1134/S0001433812040068
39. *Dolin L.S.*, *Savel'ev V.A.* Theory of the propagation of a narrow light beam in a stratified scattering medium. *Radiophysics and Quantum Electronics*. 1979, 22, 11, 911–917.
40. *Levin I.M.*, *Kopelevich O.V.* Correlations between the inherent hydrooptical characteristics in the spectral range close to 550 nm. *Oceanology*. 2007, 47, 3, 344–349. doi:10.1134/S000143700703006X
41. *Levin I.M.* Few-parameter optical models of seawater inherent optical properties. *Fundamental and Applied Hydrophysics*. 2014, 7, 3, 3–22 (in Russian).
42. *Turlaev D.G.*, *Dolin L.S.* On observing underwater objects through a wavy water surface: a new algorithm for image correction and laboratory experiment. *Izvestiya*, *Atmospheric and Oceanic Physics*. 2013, 49, 3, 339–345. doi:10.1134/S0001433813030158
43. *Turlaev D.G.* Determining the vector of slopes of the water surface from its image undernatural iilumination. *Fundamental and Applied Hydrophysics*. 2018, 11, 3, 91–96 (in Russian). doi:10.7868/S20736673180300115

## Литература

1. *Долин Л.С.*, *Савельев В.А.* О характеристиках сигнала обратного рассеяния при импульсном облучении мутной среды узким направленным световым пучком // Известия АН СССР. Физика атмосферы и океана. 1971. Т. 7, № 5. С. 505–510.
2. *Браво-Животовский Д.М.*, *Гордеев Л.Б.*, *Долин Л.С.*, *Моченев С.Б.* Определение показателей поглощения и рассеяния морской воды по некоторым характеристикам светового поля искусственных источников света // Гидрофизические и гидрооптические исследования в Атлантическом и Тихом океанах. Под ред. А.С. Монина, К.С. Шифрина. М.: Наука, 1974. С. 153–158.
3. Оптика океана / Под ред. А.С. Монина. М.: Наука, 1983. Т. 1. Физическая оптика океана. 371 с.
4. *Billard B.*, *Abbot R.H.*, *Penny M.F.* Airborne estimation of sea turbidity parameters from the WRELANDS laser airborne depth sounder // Applied Optics. 1986. Vol. 25. P. 2080–2088.
5. *Браво-Животовский Д.М.*, *Долин Л.С.*, *Савельев В.А.*, *Фадеев В.В.*, *Щегольков Ю.Б.* Оптические методы диагностики океана. Лазерное дистанционное зондирование // «Дистанционные методы изучения океана». Горький: ИПФ АН СССР, 1987. С. 84–125.
6. *Hoge F.E.*, *Wright C.W.*, *Krabill W.B.*, *Buntzen R.R.*, *Gilbert G.D.*, *Swift R.N.*, *Yungel J.K.*, *Berry R.E.* Airborne lidar detection of subsurface oceanic scattering layers // Applied Optics. 1988. Vol. 27. P. 3969–3977.
7. *Васильков А.П.*, *Кондранин Т.В.*, *Мясников Е.В.* Определение профиля показателя рассеяния света по поляризационным характеристикам отраженного назад излучения при импульсном зондировании океана. // Известия АН СССР, Физика атмосферы и океана. 1990. Т. 26, № 3. С. 307–312.
8. *Долин Л.С.*, *Левин И.М.* Справочник по теории подводного видения. Ленинград: Гидрометеоиздат, 1991. 230 с.
9. *Dolin L.S.*, *Levin I.M.* Optics, Underwater // Encyclopedia of Applied Physics, VCH Publishers, 1995. Vol. 12. P. 571–601.
10. *Васильков А.П.*, *Гольдин Ю.А.*, *Гуреев Б.А.* Определение вертикального распределения показателя рассеяния морской воды с помощью авиационного поляризационного лидара // Известия РАН. Физика атмосферы и океана. 1997. Т. 33, № 4. С. 563–569.
11. *Vasilkov A.P.*, *Goldin Y.A.*, *Gureev B.A.*, *Hoge F.E.*, *Swift R.N.*, *Wright C.W.* Airborne polarized lidar detection of scattering layers in the ocean // Applied Optics. 2001. Vol. 40, N 24. P. 4353–4364. doi:10.1364/AO.40.004353

12. *Bissonnette L.R.*, *Roy G.*, *Poutier L.*, *Cober S.G.*, *Isaac G.A.* Multiple-scattering lidar retrieval method: tests on Monte Carlo simulations and comparisons with *in situ* measurements // Applied Optics. 2002. Vol. 41, N 30. P. 6307–6324. doi:10.1364/AO.41.006307
13. *Feygels V.I.*, *Kopilevich Y.I.*, *Surkov A.*, *Yangel J.K.*, *Behrenfeld M.J.* Airborne lidar system with variable field-of-view receiver for water optical measurements // Proceedings of SPIE. Ocean Remote Sensing and Imaging II. 2003. Vol. 5155. P. 12–21.
14. *Коханенко Г.П.*, *Крекова М.М.*, *Пеннер И.Э.*, *Шаманаев В.С.* Обнаружение неоднородностей гидрозоля поляризационным лидаром // Оптика атмосферы и океана. 2004. Т. 17, № 9. С. 750–758.
15. *Kopilevich Yu.*, *Feygels V.I.*, *Tuell G.H.*, *Surkov A.* Measurement of ocean water optical properties and seafloor reflectance with scanning hydrographic operational airborne lidar survey (SHOALS): I. Theoretical background // Proceedings of SPIE. 2005. Vol. 5885. 9 p.
16. *Tuell G.H.*, *Feygels V.*, *Kopilevich Yu.*, *Weidemann A.D.*, *Cunningham A.G.*, *Mani R.*, *Podoba V.*, *Ramnath V.*, *Park J.Y.*, *Aitken J.* Measurement of ocean water optical properties and seafloor reflectance with scanning hydrographic operational airborne lidar survey (SHOALS): II. Practical results and comparison with independent data // Proceedings of SPIE. 2005. Vol. 5885. 13 p.
17. *Hoge F.E.* Oceanic inherent optical properties: proposed single laser lidar and retrieval theory // Applied Optics. 2005. Vol. 44, N 34. P. 7483–7486. doi:10.1364/AO.44.007483
18. *Churnside J.H.*, *Thorne R.E.* Comparison of airborne lidar measurements with 420 kHz echo-sounder measurements of zooplankton // Applied Optics. 2005. Vol. 44, N 26. P. 5504–5514. doi:10.1364/AO.44.005504
19. *Zege E.*, *Katsev I.*, *Prikhach A.* Retrieval of seawater inherent optical properties profiles from lidar waveforms // Proceedings of SPIE. 2007. Vol. 6615, 66150B, 10 p.
20. *Dolina I.S.*, *Dolin L.S.*, *Levin I.M.*, *Rodionov A.A.*, *Savel'ev V.A.* Inverse problems of lidar sensing of the ocean. In: Current Research on Remote Sensing, Laser Probing, and Imagery in Natural Waters // Proceeding of SPIE. 2007. Vol. 6615, 66150C — 1–10.
21. *Долин Л.С.* Лидарный метод измерения частотно-контрастной характеристики водных слоев // Фундаментальная и прикладная гидрофизика. 2010. Т. 3, № 3 (9). С. 62–71.
22. *Коханенко Г.П.*, *Балин Ю.С.*, *Пеннер И.Э.*, *Шаманаев В.С.* Лидарные и in situ измерения оптических параметров поверхностных слоев воды в озере Байкал // Оптика атмосферы и океана. 2011. Т. 24, № 5. С. 377–385.
23. *Palmer S.C.J.*, *Pelevin V.V.*, *Goncharenko I.*, *Kovács A.W.*, *Zlinszky A.*, *Présing M.*, *Horváth H.*, *Nicolás-Perea V.*, *Balzter H.*, *Tóth V.R.* Ultraviolet Fluorescence LiDAR (UFL) as a Measurement Tool for Water Quality Parameters in Turbid Lake Conditions // Remote Sensing. 2013. Vol. 5. P. 4405–4422. doi:10.3390/rs5094405
24. *Пелевин В.В.*, *Завьялов П.О.*, *Коновалов Б.В.*, *Абрамов О.И.*, *Грабовский А.Б.*, *Гончаренко И.В.* Дистанционное лазерное зондирование морей и внутренних водоемов портативными ультрафиолетовыми лидарами // Труды VIII международной конференции «Современные проблемы оптики естественных вод». 2015. С. 179–184.
25. *Глухов В.А.*, *Гольдин Ю.А.*, *Родионов М.А.* Экспериментальная оценка возможностей лидара ПЛД-1 по регистрации гидрооптических неоднородностей в толще морской среды // Фундаментальная и прикладная гидрофизика. 2017. Т. 10, № 2. С. 41–48. doi:10.7868/S207366731702006X
26. *Глухов В.А.*, *Гольдин Ю.А.*, *Родионов М.А.* Лидарный метод регистрации внутренних волн в водах с двухслойной стратификацией гидрооптических характеристик // Фундаментальная и прикладная гидрофизика. 2021. Т. 14, № 3. С. 86–97. doi:10.7868/S2073667321030084
27. *Леднёв В.Н.*, *Гришин М.Я.*, *Першин С.М.*, *Бункин А.Ф.*, *Капустин И.А., Мольков А.А., Ермаков С.А.* Лидарное зондирование пресноводной акватории с высокой концентрацией фитопланктона // Современные проблемы дистанционного зондирования Земли из Космоса. 2016. Т. 13, № 1. С. 119–134. doi:10.21046/2070-7401-2016-13-1-119-134
28. *Grishin M. Ya.*, *Lednev V.N.*, *Pershin S.M.*, *Bunkin A.F.*, *Kobylyanskiy V.V.*, *Ermakov S.A.*, *Kapustin I.A.*, *Molkov A.A.* Laser remote sensing of an algal bloom in a freshwater reservoir // Laser Physics. 2016. Vol. 26. 125601 (8pp). doi:10.1088/1054–660X/26/12/125601
29. *Мольков А.А.*, *Капустин И.А.*, *Щегольков Ю.Б.*, *Воденеева Е.Л.*, *Калашников И.Н.* Взаимосвязь первичных гидрооптических характеристик на 650 нм с глубиной видимости диска Секки и концентрацией сине-зеленых водорослей в Горьковском водохранилище // Фундаментальная и прикладная гидрофизика. 2018. Т. 11, № 3. С. 26–33. doi:10.7868/S2073667318030036
30. *Molkov A.A., Fedorov S.V.*, *Pelevin V.V.*, *Korchemkina E.N.* On regional models for high-resolution retrieval of Chlorophyll a and TSM Concentrations in the Gorky Reservoir by Sentinel-2 Imagery // Remote Sensing. 2019. Vol. 10, N 11. P. 1215–1241. doi.org/10.3390/rs11101215

31. *Мольков А.А., Пелевин В.В., Корчемкина Е.Н.* Оригинальная методика валидации спутниковых данных в условиях сильной пространственно-временной изменчивости оптических свойств воды внутренних эвтрофных водоемов // Фундаментальная и прикладная гидрофизика. 2020. Т. 13, № 2. С. 60–67. doi:10.7868/S2073667320020070
32. *Fukshansky L.* Absorption statistics in turbid media // Journal of Quantitative Spectroscopy and Radiative Transfer. 1987. Vol. 38. P. 389–406.
33. *McClendon J.H.*, *Fukshansky L.* On the interpretation of absorption spectra of leaves — II. The non-absorbed ray of the sieve effect and the mean optical pathlength in the remainder of the leaf // Photo-chem Photobiol. 1990. Vol. 51. P. 211–216.
34. *Anisimov O.*, *Fukshansky L.* Stochastic radiation in macroheteroge-neous random optical media // Journal of Quantitative Spectroscopy and Radiative Transfer. 1992. Vol. 48. P. 169–186.
35. *Долин Л.С.*, *Сергеева Е.А.*, *Турчин И.В.* Теневые шумы в оптических томограммах биотканей // Квантовая электроника. 2008. Т. 38, № 6. С. 543–550.
36. *Долин Л.С.* Развитие теории переноса излучения в приложении к задачам инструментального видения в мутных средах // Успехи физических наук. 2009. Т. 179, № 5. С. 553–560. doi:10.3367/UFNe.0179.200905k.0553
37. *Dolin L.S.*, *Sergeeva E.A.*, *Turchin I.V.* Correlation characteristics of optical coherence tomography images of turbid media with statistically inhomogeneous optical parameters // Journal of Quantitative Spectroscopy and Radiative Transfer. 2012. Vol. 113, N 9. P. 691–703. doi:10.1016/j.jqsrt.2012.02.004
38. *Долин Л.С.*, *Долина И.С.*, *Савельев В.А.* Лидарный метод определения характеристик внутренних волн // Известия РАН. Физика атмосферы и океана. 2012. Т. 48, № 4. С. 501–511.
39. *Долин Л.С.*, *Савельев В.А.* К теории распространения узкого пучка света в стратифицированной рассеивающей среде // Известия вузов. Радиофизика. 1979. Т. 22, № 11. С. 1310–1317.
40. *Левин И.*, *Копелевич О.* Корреляционные соотношения между первичными гидрооптическими характеристиками в спектральном диапазоне около 550 нм. // Океанология. 2007. № 3, С. 374–379.
41. *Левин И.М.* Малопараметрические модели первичных оптических характеристик морской воды // Фундаментальная и прикладная гидрофизика. 2014. Т. 7, № 3, С. 3–22.
42. *Турлаев Д.Г., Долин Л.С.* О наблюдении подводных объектов через взволнованную водную поверхность: новый алгоритм коррекции изображений и лабораторный эксперимент // Изв. РАН. Физика атмосферы и океана. 2013. Т. 49, № 3. С. 370–376.
43. *Турлаев Д.Г.* Нахождение вектора уклонов взволнованной водной поверхности по ее изображению в условиях естественного освещения // Фундаментальная и прикладная гидрофизика. 2018. Т. 11, № 3. С. 91–96. doi:10.7868/S20736673180300115

## About the author

**DOLIN Lev Sergeevich**, РИНЦ Author ID: 18674, ORCID ID: 0000-0002-0043-8972,
Scopus Author ID: 7003454310, lev.dolin@ipfran.ru